Quantification of the Thermodynamically Linked Quaternary and Tertiary Structural Stabilities of Transthyretin and Its Disease-Associated Variants: The Relationship between Stability and Amyloidosis[†]

Amy R. Hurshman Babbes,[‡] Evan T. Powers,*[,§] and Jeffery W. Kelly*[,§]

Joint Science Department, Claremont McKenna, Pitzer, and Scripps Colleges, 925 North Mills Avenue, Claremont, California 91711, and Department of Chemistry and Skaggs Institute for Chemical Biology, The Scripps Research Institute, 10550 North Torrey Pines Road, BCC265, La Jolla, California 92037

Received April 9, 2008; Revised Manuscript Received May 8, 2008

ABSTRACT: Urea denaturation studies were carried out as a function of transthyretin (TTR) concentration to quantify the thermodynamically linked quaternary and tertiary structural stability and to improve our understanding of the relationship between mutant folding energetics and amyloid disease phenotype. Urea denaturation of TTR involves at least two equilibria: dissociation of tetramers into folded monomers and monomer unfolding. To deal with the thermodynamic linkage of these equilibria, we analyzed concentration-dependent denaturation data by globally fitting them to an equation that simultaneously accounts for the two-step denaturation process. Using this method, the quaternary and tertiary structural stabilities of well-behaved TTR sequences, wild-type (WT) TTR and the disease-associated variant V122I, were scrutinized. The V122I variant is linked to late onset familial amyloid cardiomyopathy, the most common familial TTR amyloid disease. V122I TTR exhibits a destabilized quaternary structure and a stable tertiary structure relative to those of WT TTR. Three other variants of TTR were also examined, L55P, V30M, and A25T TTR. The L55P mutation is associated with the most aggressive familial TTR amyloid disease. L55P TTR has a complicated denaturation pathway that includes dimers and trimers, so globally fitting its concentration-dependent urea denaturation data yielded error-laden estimates of stability parameters. Nevertheless, it is clear that L55P TTR is substantially less stable than WT TTR, primarily because its tertiary structure is unstable, although its quaternary structure is destabilized as well. V30M is the most common mutation associated with neuropathic forms of TTR amyloid disease. V30M TTR is certainly destabilized relative to WT TTR, but like L55P TTR, it has a complex denaturation pathway that cannot be fit to the aforementioned two-step denaturation model. Literature data suggest that V30M TTR has stable quaternary structure but unstable tertiary structure. The A25T mutant, associated with central nervous system amyloidosis, is highly aggregation-prone and exhibits drastically reduced quaternary and tertiary structural stabilities. The observed differences in stability among the disease-associated TTR variants highlight the complexity and heterogeneity of TTR amyloid disease, an observation that has important implications for the treatment of these maladies.

Transthyretin (TTR)[1] is one of more than 30 amyloidogenic proteins that, when partially denatured, can misassemble into several aggregate structures, including cross-β sheet amyloid fibril quaternary structures (*1–6*). The process of amyloidogenesis is causatively linked to numerous human diseases, many of which are associated with neurodegeneration (*1–3*). To date, all of the TTR variants associated with familial amyloidosis that have had their folding energetics characterized, 21 of them, are destabilized relative to WT TTR, based on the observation that their denaturation transitions occur at lower concentrations of urea than those of WT TTR (*7–15*). TTR is tetrameric under physiological conditions. The thermodynamic linkage of the TTR tetramer dissociation and monomer unfolding equilibria makes it challenging to extract thermodynamic data from the urea denaturation curves (*7*). How disease-associated mutations influence quaternary and tertiary structural stability and how folding and tetramerization energetics correlate with disease phenotypes are some of the valuable insights sought herein.

Generally, rate-limiting tetramer dissociation enables monomer misfolding that is required for TTR to form amyloid (*5, 16–22*), by a very efficient downhill polymeri-

[†] This research was supported by NIH Grant DK46335, the Skaggs Institute for Chemical Biology, and the Lita Annenberg Hazen Foundation. A.R.H.B. was supported by NIH Grants T32-AG00080 and F32-GM067348.

* To whom correspondence should be addressed. Phone: (858) 784-9601. Fax: (858) 784-9610. E-mail: epowers@scripps.edu or jkelly@scripps.edu.

[‡] Claremont McKenna, Pitzer, and Scripps Colleges.

[§] The Scripps Research Institute.

[1] Abbreviations: TTR, transthyretin; WT, wild-type; M-TTR, monomeric variant of transthyretin harboring F87M and L110M mutations; SSA, senile systemic amyloidosis; FAP, familial amyloid polyneuropathy; FAC, familial amyloid cardiomyopathy; Tris, tris(hydroxymethyl)aminomethane; EDTA, ethylenediamine-*N*,*N*,*N*′,*N*′-tetraacetic acid; DTT, dithiothreitol; SDS−PAGE, sodium dodecyl sulfate−polyacrylamide gel electrophoresis; CSF, cerebrospinal fluid.

10.1021/bi800636q CCC: $40.75
Published on Web 06/07/2008

zation process (*23*). Most of the disease-associated TTR mutant proteins form normal tetrameric structures based on crystallographic analysis (*24*) and function normally, including binding and transporting thyroid hormone and holoretinol binding protein in the plasma and cerebrospinal fluid (CSF). Thus, it is the propensity of these variants to misfold, not their inability to fold and function, that results in disease through a gain-of-toxic-function mechanism(s), the details of which remain elusive but appear to be associated with TTR aggregation (*7, 17, 18, 25, 26*).

Senile systemic amyloidosis (SSA) is a disease that typically presents after age 60, characterized by the deposition of WT TTR in the heart, ultimately leading to congestive heart failure (*27*). SSA appears to affect as much as 25% of the population that is more than 80 years old (*27*). A number of autosomal dominant TTR amyloidoses have also been described that are associated with the deposition of variant transthyretin. These disorders have been subcategorized as familial amyloid polyneuropathy (FAP), familial amyloid cardiomyopathy (FAC), and central nervous system selective amyloidosis (CNSA), depending on the tissue(s) affected by deposition of the mutant TTR proteins (*8, 12, 13, 28, 29*).

The liver secretes TTR into the blood, whereas the choroid plexus secretes TTR into the CSF; secreted TTR from the liver and the choroid appears to be the source of amyloidogenic transthyretin in the periphery and brain, respectively. Gene therapy mediated via replacement of a disease-associated variant TTR/WT TTR-expressing liver with a WT TTR/WT TTR-expressing liver through transplantation has proven to be a useful strategy for treating familial amyloid polyneuropathy (*30*). We have discovered small molecule TTR tetramer binders that impose kinetic stability on the tetramer, preventing dissociation required for amyloidogenesis (*20, 31–34*). Two such small molecules are currently being tested as agents to ameliorate FAP in placebo-controlled clinical trials (see http://www.clinicaltrials.gov/). This approach is expected to be efficacious because kinetic stabilization of tetrameric transthyretin containing disease-associated subunits by interallelic trans suppression (the incorporation of T119M TTR subunits) ameliorates FAP (*17, 18, 20, 35*).

Since TTR tetramer dissociation, partial monomer denaturation, and amyloidogenesis are associated with several familial gain-of-function proteotoxicity diseases, we set out to examine the correlation between the quaternary and tertiary structural stabilities of TTR and disease phenotype. Folding and association energetics can be quantified by globally fitting chaotrope denaturation data obtained at several protein concentrations (*36–40*). Systematic urea denaturation studies were therefore carried out as a function of the concentration of TTR. These data corroborated our previous report that the tetramer dissociation and monomer unfolding equilibria are thermodynamically linked (*7*). For well-behaved TTR sequences, we analyzed the concentration-dependent denaturation data by globally fitting them to an equation that simultaneously accounts for the two-step denaturation process (tetramer to folded monomer and folded monomer to unfolded monomer). The concentration-dependent denaturation data for less-well behaved variants were analyzed qualitatively. Quantitative and qualitative analysis of the denaturation data, combined with literature reports on TTR folding energetics, reveals that each TTR variant has a unique stability profile that can be used to rationalize their disease phenotypes by considering how their folding energetics influence factors like their in vivo aggregation propensities and their interaction with the endoplasmic reticulum-associated degradation (ERAD) machinery (*13, 41*).

EXPERIMENTAL PROCEDURES

Expression and Purification of TTR. All TTR variants were expressed in BL21(DE3) Epicurian Gold *Escherichia coli* cells (Stratagene, La Jolla, CA), transformed with the appropriate pMMHa expression vector containing the TTR and ampicillin resistance genes (*42*). *E. coli* cultures were grown, harvested, and lysed in the presence of protease inhibitors, and the cell lysates were centrifuged, as previously described (*23*). All of the variants examined were expressed as soluble proteins and were therefore purified from cell supernatants.

(a) Tetrameric TTR Variants (WT TTR, V30M, L55P, V122I, and A25T). The supernatant was fractionated by ammonium sulfate precipitation; the 50−100% ammonium sulfate pellet was resuspended in a minimal volume of 25 mM Tris and 1 mM EDTA (pH 8.0) and was dialyzed in 10000 molecular weight cutoff (MWCO) dialysis tubing (Snakeskin from Pierce Biotechnology, Rockford, IL) against 4 L of 25 mM Tris and 1 mM EDTA (pH 8.0) overnight at 4 °C. After dialysis, the sample was filtered through 0.22 μm filters and applied to a Source 15Q anion exchange column (Amersham Biosciences, Piscataway, NJ), which had been equilibrated with 25 mM Tris, 1 mM EDTA, and 50 mM NaCl (pH 8.0) and was run at 4 °C. TTR was eluted with a linear gradient from 50 to 350 mM NaCl in 1.5 column volumes followed by a 350 mM NaCl wash for 1.5 column volumes. Fractions containing TTR (the major peak in all cases) were pooled, concentrated, and further purified on a Superdex 75 gel filtration column (Amersham Biosciences) in 50 mM sodium phosphate, 100 mM KCl, and 1 mM EDTA (pH 7.4) at 4 °C, to remove any soluble TTR aggregates. The identity of each purified TTR variant was confirmed by its mass, determined by electrospray liquid chromatography and mass spectroscopy (LC−MS) on a HP Series 1100-MSD liquid chromatography/mass spectrometer (Agilent Technologies, Palo Alto, CA), as previously described (*8*). The masses determined for each TTR protein (WT TTR, 13890 Da; V122I, 13904 Da; L55P, 13874 Da; V30M, 13922 Da; A25T, 13920 Da; M-TTR, 13892 Da) are consistently ~2 Da lower than the calculated values, which include the expected extra N-terminal Met present in all of our recombinant TTR variants. Concentrations of TTR solutions are expressed in micromolar units and were determined spectrophotometrically, using an ϵ_{280} of 1.88×10^4 M^{-1} cm^{-1}. A typical purification yields 60−100 mg of tetrameric TTR from 2 L of cell culture. All TTR solutions were stored at 4 °C and were used within a week of purification, except for solutions of the aggregation-prone A25T variant, which were used immediately following purification.

(b) Monomeric TTR Variant (M-TTR). M-TTR was purified using the procedure described above, with slight modifications to the ammonium fractionation step. A 25 to 90% ammonium sulfate pellet was obtained, resuspended, and dialyzed in 3500 MWCO Snakeskin dialysis tubing

(Pierce Biotechnology). The typical yield is 40−60 mg of M-TTR from 2 L of cell culture; M-TTR thus obtained is >95% monomeric, as previously reported (*19, 23*).

Urea Denaturation. Stock solutions of urea were prepared in buffer, with final concentrations of ~10 M urea, 50 mM sodium phosphate, 100 mM KCl, 1 mM EDTA, and 1 mM DTT (pH 7.4); the exact concentration of urea was determined from refractive index measurements (*43*). Denaturation reaction mixtures (total volume of 200 μL) containing varying concentrations of TTR (0.72−144 μM) and urea (0−8 M) in 50 mM sodium phosphate, 100 mM KCl, 1 mM EDTA, and 1 mM DTT (pH 7.4) were incubated for 96 h at 4 °C, unless otherwise noted. This incubation time was found previously to be sufficient for the samples to reach equilibrium (*44*), with the exception of V30M (see Results and Discussion); incubation times of >96 h were avoided, because they resulted in some urea-mediated covalent modifications of TTR, as previously reported (*44*). After 96 h, the samples were removed from the cold room and equilibrated for 1 h at 25 °C prior to the acquisition of fluorescence data. For each TTR variant, denaturation curves were obtained at seven different TTR concentrations. Each denaturation curve, at a given TTR concentration, was derived from 20 separate denaturation reactions at different urea concentrations, to accurately define the pre- and post-transition baselines and the transition region of each curve.

Renaturation Experiments. For some experiments, TTR was first completely denatured at a high urea concentration and then allowed to undergo renaturation triggered by dilution of the chaotrope. TTR was concentrated in centrifugal filters (Centriprep or Microcon from Millipore Corp., Billerica, MA; 10000 MWCO for tetrameric TTR variants and 3000 MWCO for M-TTR) to the desired concentration and filtered or spun to remove any aggregates. Denaturation reaction mixtures containing 8 M urea and TTR at high concentrations (360−720 μM) were incubated for 96 h at 4 °C in 50 mM sodium phosphate buffer (pH 7.4), containing 100 mM KCl, 1 mM EDTA, and 1 mM DTT. After 96 h, complete denaturation was verified using intrinsic tryptophan fluorescence, and renaturation assays were initiated by dilution of the denatured TTR sample into buffer containing varying concentrations of urea (up to 8 M). The lowest concentration of urea achievable in the renaturation reactions depended on the exact experiment but was always >0 M, due to the presence of urea in the denatured TTR sample. Reaction mixtures were incubated for an additional 24 h at 25 °C to allow complete refolding of TTR monomers and reassembly of TTR tetramers (renaturation) prior to fluorescence measurements.

Tertiary Structure Assessed by Tryptophan Fluorescence. The extent of unfolding of TTR was evaluated by intrinsic protein fluorescence spectroscopy (*44*). Samples were excited at 295 nm (2 nm bandwidth), and fluorescence emission spectra were recorded from 310 to 410 nm (6 nm bandwidth) at 1 nm intervals with an averaging time of 0.3 s on an AVIV ATF-105 fluorometer (AVIV Instruments, Lakewood, NJ). This excitation wavelength was chosen to allow selective excitation of the tryptophan residues in TTR (Trp41 and Trp79). Upon denaturation, these tryptophan residues become more solvent-exposed, and $\lambda_{max,emission}$ shifts from ~335 nm in the native state to ~355 nm in the unfolded state; the tryptophan emission spectrum is therefore a sensitive probe of the tertiary structure of TTR. Spectra were corrected by subtraction of a buffer blank, and the fluorescence intensities at 335 and 355 nm were recorded for each sample. The ratio of the fluorescence intensities at these two wavelengths (F_{355}/F_{335}) was used as a measure of the extent of tertiary structure unfolding, to allow direct comparisons of the various denaturation curves. For all of the tetrameric TTR variants, the F_{355}/F_{335} ratio for the native state in the absence of urea is ~0.85, and that of the denatured state in the presence of 8 M urea is 1.3−1.35. The F_{355}/F_{335} ratios for M-TTR are similar to those of the tetrameric variants, with the ratio for the native state in the absence of urea consistently being slightly lower, ~0.82.

Quaternary Structure Assessed by Resveratrol Binding. The binding of the small molecule resveratrol to the TTR tetramer was used to assess the quaternary structure of TTR as a function of urea concentration and TTR concentration, as previously described (*7, 12*). Resveratrol binding to tetrameric TTR (occupying at least one of the two thyroxine-binding sites) results in a blue shift in the fluorescence spectrum of resveratrol and a concomitant large increase in its fluorescence quantum yield. In contrast, studies with M-TTR have shown that resveratrol does not bind to monomeric TTR (X. Jiang and J. W. Kelly, unpublished results). An aliquot (1.44 μL) of a stock solution of resveratrol (0.5−12.5 mM in DMSO) was added to denatured TTR samples (200 μL containing 1.44, 7.2, or 36 μM TTR) immediately prior to fluorescence measurements, to minimally perturb the slowly attained tetramer−monomer equilibrium. The final concentration of resveratrol (3.6, 18, or 90 μM) varied according to the concentration of TTR and was present in each assay at a 10-fold stoichiometric excess over the maximum concentration of TTR tetramer (1.44 μM monomer = 0.36 μM tetramer; 36 μM monomer = 9.0 μM tetramer). Fluorescence emission spectra were recorded from 350 to 550 nm (5 nm bandwidth, 1 nm data interval, 0.3 s averaging time) on an AVIV ATF-105 fluorometer (AVIV Instruments), with an excitation wavelength of 320 nm (2 nm bandwidth). Spectra were corrected by subtraction of a buffer blank, and the fluorescence intensities at 390 nm (F_{390}) were used directly as a measure of the amount of tetramer present in each sample.

Quaternary Structure Assessed by Glutaraldehyde Cross-Linking and SDS−PAGE. To independently assess the TTR quaternary structural changes quantified by resveratrol fluorescence, glutaraldehyde cross-linking was also employed. Glutaraldehyde [5 μL of a 25% (w/w) solution in water, from Sigma-Aldrich, St. Louis, MO] was added to 50 μL aliquots of TTR samples in variable concentrations of urea (containing 7.2, 36, or 144 μM TTR), and the cross-linking reaction was allowed to proceed for 4 min at room temperature prior to being quenched with $NaBH_4$ [5 μL of a 7% (w/w) solution made in 0.1 M NaOH]. Samples were immediately mixed with SDS reducing sample loading buffer, boiled for 5 min, and analyzed by discontinuous SDS−PAGE (3.9% acrylamide stacking gel, 12% acrylamide separating gel). A25T samples were run on gradient gels (Novex 10 to 20% Tris-glycine precast gels from Invitrogen, Carlsbad, CA) to allow visualization of high-molecular weight aggregates present in those samples. The total protein loaded in each lane was ~1.8 μg for the A25T samples and ~1.0 μg for all other samples. Gels were stained with

colloidal Coomassie Blue G-250 (GelCode Blue Stain Reagent from Pierce Biotechnology), and protein bands were identified by comparison to molecular weight standards (BenchMark Prestained Protein Ladder from Invitrogen). After being stained, the gels were scanned, and the bands were quantified by densitometry, using NIH Image (National Institutes of Health; http://rsb.info.nih.gov/nih-image).

Data Analysis. Denaturation curves were plotted, and stabilities of TTR were determined by fitting the data to a two-state model for either tetramer dissociation or monomer unfolding in the presence of urea.

(a) Determination of Apparent C_m Values for Monomer Unfolding ($C_{m,unfold}$). The midpoint urea concentration values for monomer unfolding ($C_{m,unfold}$) were determined by fitting individual tryptophan fluorescence denaturation curves to the following equation (*45*):

$$y = \{\alpha_{folded} + \beta_{folded}[urea] + (\alpha_{unfolded} + \beta_{unfolded}[urea]) \times \exp[m_{unfold}([urea] - C_{m,unfold})/RT]\}/\{1 + \exp[m_{unfold}([urea] - C_{m,unfold})/RT]\} \quad (1)$$

where y is the observed signal (F_{355}/F_{335} in this case), α_{folded} is the y-intercept, and β_{folded} is the slope of the pretransition baseline, which describes the F_{355}/F_{335} value of folded TTR monomer or tetramer at a given concentration of urea; $\alpha_{unfolded}$ is the y-intercept and $\beta_{unfolded}$ is the slope of the post-transition baseline, describing the F_{355}/F_{335} value of the unfolded monomer at a given concentration of urea; $C_{m,unfold}$ and m_{unfold} describe the transition region of the denaturation curve, with $C_{m,unfold}$ corresponding to the urea concentration where the protein is 50% unfolded (molar urea) and m_{unfold} to the constant of proportionality relating the free energy of unfolding to the urea concentration (kilocalories per mole per molar urea); and R is the universal gas constant (kilocalories per kelvin per mole) and T is the absolute temperature (kelvin). $C_{m,unfold}$ values thus determined were used either for comparisons of apparent stability of single variants as a function of TTR concentration, or for comparisons of apparent stability among all TTR variants examined at the same protein concentration. Apparent unfolding free energies ($\Delta G_{unfold,app}^{H_2O}$) were calculated from these fits by multiplying $C_{m,unfold}$ by $-m_{unfold}$.

(b) Determination of Apparent C_m Values for Tetramer Dissociation ($C_{m,diss}$). Equation 1 was slightly modified to analyze the native tetramer−folded monomer equilibrium, measured either by resveratrol binding or by glutaraldehyde cross-linking, as follows:

$$y = \{\alpha_{tetramer} + \beta_{tetramer}[urea] + (\alpha_{monomer} + \beta_{monomer}[urea]) \times \exp[m_{diss}([urea] - C_{m,diss})/RT]\}/\{1 + \exp[m_{diss}([urea] - C_{m,diss})/RT]\} \quad (2)$$

where $\alpha_{tetramer}$ and $\beta_{tetramer}$ describe the pretransition baseline, $\alpha_{monomer}$ and $\beta_{monomer}$ describe the post-transition baseline, and $C_{m,diss}$ (molar urea) and m_{diss} (kilocalories per mole per molar urea) describe the transition region of each denaturation curve. For resveratrol binding data, the blank-subtracted fluorescence intensities at 390 nm were used as the observed signal, y. For analysis of cross-linking data, the percent tetramer and percent monomer values derived from densitometry of the various samples were each plotted as a function of urea concentration, and both curves were fit separately to eq 2. $C_{m,diss}$ values derived from both measurements (percent tetramer and percent monomer) were generally in good agreement, except in cases where intermediates were detected (dimers and trimers for L55P and aggregates for A25T; see Results and Discussion).

(c) Global Fitting of Concentration-Dependent Data to Extract Thermodynamic Parameters for TTR Variants. Fraction unfolded (F_{unfold}) values for all TTR variants were calculated as follows. The blank-corrected fluorescence intensity at 355 nm was subtracted from that at 335 nm for each sample, and these values ($F_{335} - F_{355}$) were normalized for each denaturation curve to a value of 1.0 for the spectrum of native WT TTR in the absence of urea. This transformation retains the linear dependence of the fluorescence signal of the folded and unfolded states of the protein on denaturant concentration and yielded $F_{335} - F_{355}$ values ranging from 1.0 at 0 M urea to approximately −1.8 at 8 M urea (−2.0 for M-TTR). Pre- and post-transition baselines (corresponding to the signal for 100% folded monomer and 100% unfolded monomer, respectively) were determined from this data by plotting the $F_{335} - F_{355}$ values versus urea concentration and then fitting the linear portions of the plots at low and high urea concentrations to lines. The fraction of unfolded TTR (F_{unfold}) was calculated at each urea concentration in the transition region, where $F_{unfold} = (y_{sample} - y_{100\%folded})/(y_{100\%unfolded} - y_{100\%folded})$, where $y_{100\%folded}$ is the pretransition baseline and $y_{100\%unfolded}$ is the post-transition baseline.

For each variant, the F_{unfold} values determined over a range of TTR and urea concentrations were fit globally to a three-state model comprising unfolded monomer, folded monomer, and tetramer:

$$\text{monomer}_{unfolded} \overset{K_{unfold}}{\rightleftharpoons} \text{monomer}_{folded}$$

$$4\text{monomer}_{folded} \overset{K_{diss}}{\rightleftharpoons} \text{tetramer}$$

where K_{unfold} is the equilibrium constant for monomer folding and K_{diss} is the equilibrium constant for tetramer dissociation: $K_{diss} = [\text{monomer}_{folded}]^4/[\text{tetramer}]$ (quantities in brackets are molar concentrations). ΔG_{unfold} is related to K_{unfold} via the equation $\Delta G_{unfold} = -RT \ln K_{unfold}$. Similarly, ΔG_{diss} is related to K_{diss} through the equation $\Delta G_{diss} = -RT \ln K_{diss}$. ΔG_{unfold} and ΔG_{diss} are expected to depend on urea concentration as follows: $\Delta G_{unfold} = \Delta G_{unfold}^{H_2O} - m_{unfold}[urea]$ and $\Delta G_{diss} = \Delta G_{diss}^{H_2O} - m_{diss}[urea]$, where $\Delta G_{unfold}^{H_2O}$ and $\Delta G_{diss}^{H_2O}$ are the standard state free energies of monomer unfolding and tetramer dissociation in 0 M urea, respectively. These equations can be combined to yield

$$K_{unfold} = e^{-(\Delta G_{unfold}^{H_2O} - m_{unfold}[urea])/RT} \text{ and } K_{diss} = e^{-(\Delta G_{diss}^{H_2O} - m_{diss}[urea])/RT} \quad (3)$$

The fraction of unfolded protein at a given urea and protein concentration can be calculated for given values of $\Delta G_{unfold}^{H_2O}$, m_{unfold}, $\Delta G_{diss}^{H_2O}$, and m_{diss} using the relation

$$F_{unfolded} = \frac{[\text{monomer}_{unfolded}]}{[\text{total protein}]}$$

where the numerator is the real solution of the following polynomial equation such that $0 < [\text{monomer}_{unfolded}] < [\text{total protein}]$

$$[\text{total protein}] = [\text{monomer}_{\text{unfolded}}] + [\text{monomer}_{\text{folded}}] + 4[\text{tetramer}]$$

$$= [\text{monomer}_{\text{unfolded}}](1 + K_{\text{unfold}}^{-1} + 4K_{\text{diss}}^{-1}K_{\text{unfold}}^{-4}[\text{monomer}_{\text{unfolded}}]^3)$$

$$= [\text{monomer}_{\text{unfolded}}]\{1 + e^{(\Delta G_{\text{unfold}}^{H_2O} - m_{\text{unfold}}[\text{urea}])/RT} + 4e^{[(\Delta G_{\text{diss}}^{H_2O} - m_{\text{diss}}[\text{urea}]) + 4(\Delta G_{\text{unfold}}^{H_2O} - m_{\text{unfold}}[\text{urea}])]/RT}[\text{monomer}_{\text{unfolded}}]^3\} \quad (4)$$

The F_{unfolded} values were fit by choosing initial values for $\Delta G_{\text{unfold}}^{H_2O}$, m_{unfold}, $\Delta G_{\text{diss}}^{H_2O}$, and m_{diss}, computing the sum of squared differences between the calculated and experimental F_{unfolded} data at all protein and urea concentrations, and then varying $\Delta G_{\text{unfold}}^{H_2O}$, m_{unfold}, $\Delta G_{\text{diss}}^{H_2O}$, and m_{diss} until this sum of squared differences was a minimum. Note that using the relation $\Delta G_{\text{diss}} = -RT \ln K_{\text{diss}}$ implies that ΔG_{diss} values are for a standard state in which the protein concentration is 1 M.

RESULTS AND DISCUSSION

Characterizing the quaternary and tertiary structural stability of the various TTR sequences requires that the energetics of both tetramer dissociation and monomer unfolding be examined. Methodology for examining these two equilibria has already been published: resveratrol binding for monitoring TTR tetramer dissociation (*7, 12*) and, since tryptophan fluorescence is largely unaffected by tetramerization (*19*), intrinsic tryptophan fluorescence spectroscopy for following TTR monomer unfolding (*44*) in the presence of chaotropic agents such as urea (see Scheme 1). These methods are useful for determining thermodynamic parameters for dissociation and unfolding, provided that the two equilibria can be examined independently. This is possible when conditions exist in which only the native tetramer and folded monomer are in equilibrium (and no unfolding occurs), and in which only the folded monomer and unfolded monomer are in equilibrium (and no tetramerization occurs). When this is the case, the expressions for the dissociation and unfolding equilibrium constants have the following form: $K_{\text{diss}} = 256[\text{TTR}_{\text{total}}]^3[(1 - \alpha)^4/\alpha]$, where α represents the fraction of tetrameric TTR and the equilibrium position depends on the total concentration of TTR, and $K_{\text{unfold}} = [\text{monomer}_{\text{unfolded}}]/[\text{monomer}_{\text{folded}}] = F_{\text{unfold}}/(1 - F_{\text{unfold}})$, where F_{unfold} is the fraction of unfolded TTR and the equilibrium is independent of TTR concentration.

In contrast to this ideal scenario, results from earlier denaturation studies suggest that TTR dissociation and unfolding are thermodynamically linked under the conditions typically used in these experiments (TTR concentrations of 7.2−36 μM; note that TTR concentrations are reported throughout in terms of the total monomer concentration; the maximum possible tetramer concentration is then $^1/_4$ of the total monomer concentration). In particular, it was found that the urea denaturation curves for tetramer dissociation, measured by resveratrol binding, are nearly coincident with those monitoring monomer unfolding, as assessed by intrinsic protein fluorescence, for all the TTR variants examined (WT TTR, L55P, V122I, V30M, and T119M) (*7*). Furthermore, the urea concentration required for monomer unfolding appeared to depend on the concentration of TTR (*7*), even though the equilibrium for this process should be independent of TTR concentration. These data strongly suggest that TTR tetramer stability influences the apparent stability of TTR monomers, and the true thermodynamic parameters for either of the two equilibria cannot be determined under these experimental conditions because they are linked.

Scheme 1: Thermodynamic Stability of Tetrameric TTR[a]

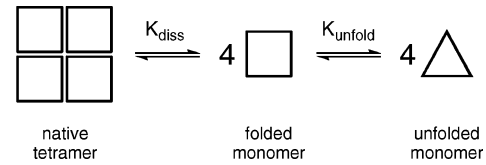

Resveratrol binding	Yes	No	No
Trp fluor λ_{max}	335 nm	335 nm	355 nm
F355/F335	~ 0.85	~ 0.85	~ 1.35

[a] Denaturation of tetrameric TTR by urea involves at least two equilibria, as shown: dissociation of the tetramer into its component monomers, which are still natively folded, and subsequent unfolding of the monomers. These equilibria are defined by the equilibrium constants K_{diss} and K_{unfold}, respectively, which can in principle be determined independently from resveratrol binding and intrinsic Trp fluorescence, respectively. The data presented herein, however, show that the equilibria for dissociation and unfolding are thermodynamically linked. When the equilibria are linked, the apparent value of K_{unfold} is dependent on TTR concentration, and the concentration dependence of K_{unfold} is a measure of the magnitude of K_{diss}. Multiple urea denaturation curves at varying TTR concentrations can hence be analyzed simultaneously to determine thermodynamic properties of both the tetramers (K_{diss}) and the monomers (K_{unfold}) of wild-type and variant TTRs. Attempts to unlink the equilibria by decreasing the concentration of TTR were unsuccessful, due to limitations in the sensitivity of the measurement techniques.

Our initial studies in this investigation focused on identifying conditions under which the equilibria could be unlinked, i.e., where the dissociation of TTR tetramers proceeds to completion (100% of TTR present as the folded monomer) at denaturant concentrations that are too low to initiate subsequent unfolding of the monomers. To achieve this goal, we tried to exploit differences in the TTR concentration dependence of the two equilibria. Whereas the equilibrium for monomer unfolding should be independent of TTR concentration, the tetramer−monomer equilibrium is highly dependent on the total concentration of TTR, as seen in the expression for K_{diss} (vide supra). A decrease in the total TTR concentration will shift this equilibrium toward the monomer, favoring dissociation and increasing the fraction of monomeric TTR present [as $[\text{TTR}_{\text{total}}]$ decreases, the $(1 - \alpha)^4/\alpha$ term concomitantly increases, which means a smaller fraction of tetrameric TTR] without affecting the unfolding equilibrium. This approach gave encouraging results but was only partially successful in unlinking the equilibria. For example, decreasing the concentration of WT TTR to 0.72 μM resulted in some separation of the C_{m} values for tetramer dissociation and monomer unfolding, determined to be 2.7 and 3.0 M urea, respectively; nevertheless, the transition regions of the two denaturation curves still overlapped significantly (data not shown). Although complete unlinking of the equilibria could in principle be achieved by decreasing the TTR concentration further, in practice this is problematic because the sensitivity of the fluorometric methods used precludes the use of TTR concentrations of less than ~0.72 μM.

An alternative approach, described herein, was used instead to determine the stabilities of TTR tetramers and monomers. Since the equilibria are thermodynamically linked, the observed dependence of the monomer unfolding equilibrium on the concentration of TTR is a measure of the stability of the TTR tetramer. In other words, not only are the denaturation curves measured by tryptophan fluorescence expected to shift to higher denaturant concentrations as the concentration of TTR is increased, as observed, but the extent to which the curves shift reflects the free energy of tetramer dissociation, with greater tetrameric stability effecting larger shifts. Therefore, global analysis of a series of tryptophan denaturation curves at varying TTR concentrations should allow the determination of the true thermodynamic parameters for both tetramer and monomer stability, provided that tetramer and monomer are the only species populated during denaturation. We describe this analysis method and its application for determination of the thermodynamic stability of wild-type TTR tetramer and monomer below. We then use this method to assess the quaternary and tertiary structural stabilities of known disease-associated variants of TTR, enabling comparisons with those parameters determined for WT TTR.

Concentration Dependence of WT TTR Denaturation. Figure 1A shows the effect of TTR concentration on the stability of WT TTR to urea denaturation, monitored by tryptophan fluorescence, for a representative experiment. Each denaturation curve was fit independently by eq 1 to a two-state denaturation model; the resulting fits are shown as curves overlaid with the corresponding data (symbols). At the lowest WT TTR concentration shown (1.44 μM), the midpoint for unfolding (or the urea concentration at which WT TTR is 50% unfolded, $C_{m,unfold}$) occurs at ~3.1 M urea, with a value of $-m_{unfold}$ (the dependence of the free energy of unfolding on urea concentration) of ~1.5 kcal mol^{-1} (M urea)$^{-1}$. As the concentration of WT TTR is increased, two obvious changes in the denaturation curves are revealed: (1) The curves shift to the right, with the apparent $C_{m,unfold}$ gradually increasing up to ~4.0 M urea at 144 μM WT TTR, and (2) the steepness of the curve in the transition region increases, which is reflected in larger apparent values of $-m_{unfold}$, up to ~3.9 kcal mol^{-1} (M urea)$^{-1}$ at WT TTR concentrations of ≥36 μM. The magnitude of $-m_{unfold}$ reflects the amount of surface area that is exposed upon unfolding (*46*). The values of $-m_{unfold}$ are large for TTR at high concentrations because tetramer dissociation and monomer unfolding are so tightly linked that the surface area exposed by these two processes is essentially combined. Tetramer dissociation and monomer unfolding are less tightly linked at lower concentrations, and the apparent $-m_{unfold}$ values are correspondingly lower. In contrast to these results, denaturation curves for M-TTR, a monomeric variant of WT TTR, exhibit no dependence on TTR concentration (Figure 1B; discussed further below).

The apparent Gibbs free energy of monomer unfolding in the absence of denaturant, $\Delta G_{unfold,app}^{H_2O}$, can be calculated by multiplying the values of $C_{m,unfold}$ and $-m_{unfold}$ obtained as described above. Calculated values of $\Delta G_{unfold,app}^{H_2O}$ range from 4.7 kcal/mol at 1.44 μM WT TTR to >15 kcal/mol at 72 and 144 μM WT TTR. We call the parameter obtained from fitting the individual denaturation curves to a two-state model an "apparent" $\Delta G_{unfold}^{H_2O}$ because TTR denaturation

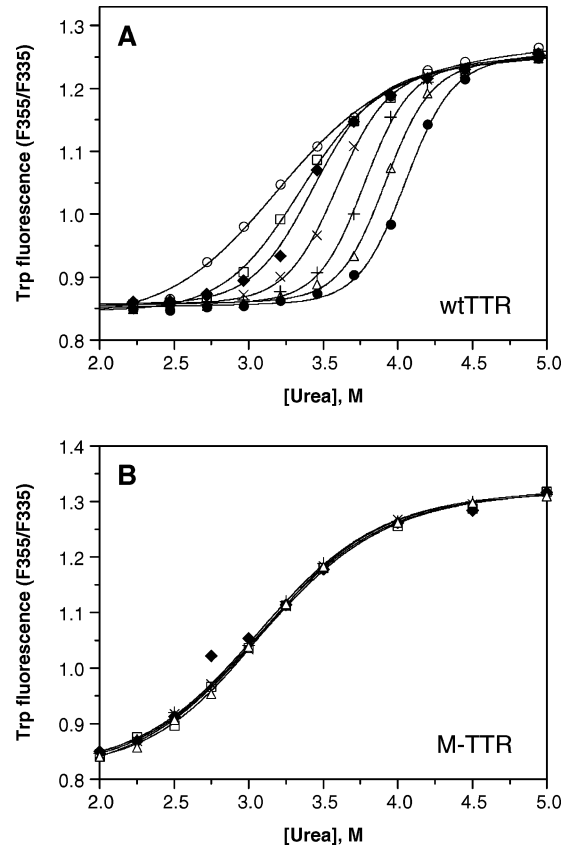

FIGURE 1: Dependence of urea denaturation of WT TTR (A) and M-TTR (B) on TTR concentration. Denaturation reaction mixtures contained TTR (1.44−144 μM) and were incubated for 96 h at 4 °C in the presence of varying concentrations of urea (0−8 M) prior to fluorescence measurements (see Experimental Procedures for details). The intrinsic tryptophan fluorescence of TTR shifts from a maximum emission wavelength of 335 nm in the native state to 355 nm upon denaturation; hence, the ratio of the fluorescence intensity at these two wavelengths (F_{355}/F_{335}) is a measure of the extent of denaturation. TTR concentrations in this representative experiment were 1.44 (○), 3.6 (□), 7.2 (◆), 14.4 (×), 36 (+), 72 (△), and 144 μM (●), and the fits of each denaturation curve to eq 1 are shown as solid lines. The apparent stability of WT TTR monomers to urea denaturation increases with an increase in TTR concentration (from $C_{m,unfold}$ = 3.1 to 4.0 M urea); in contrast, the concentration of M-TTR has no effect on its apparent stability ($C_{m,unfold}$ = 3.1 M urea at all M-TTR concentrations examined).

is a process comprising at least two steps. Since in reality we are simultaneously evaluating the tetramer dissociation and monomer unfolding equilibria, $\Delta G_{unfold,app}^{H_2O}$ is a composite stability parameter that "combines" the free energy of monomer unfolding and the free energy of tetramer dissociation. As the TTR concentration is increased, the two equilibria become more linked, and the free energy of tetramer dissociation, $\Delta G_{diss}^{H_2O}$, influences $\Delta G_{unfold,app}^{H_2O}$ to a greater extent, resulting in greater values of $\Delta G_{unfold,app}^{H_2O}$. Although we were unable to measure the folded monomer and unfolded monomer concentrations independently in these experiments, the equilibria became less tightly linked at low TTR concentrations, and hence, the $\Delta G_{unfold,app}^{H_2O}$ of 4.7 kcal/mol determined at 1.44 μM begins to approximate the true stability of the WT TTR monomer. The thermodynamic parameters ($C_{m,unfold}$, $-m_{unfold}$, and $\Delta G_{unfold,app}^{H_2O}$) calculated from these analyses of the individual tryptophan denaturation curves are summarized in Table 1.

Table 1: Apparent Stabilities of WT TTR at Varying TTR Concentrations[a]

	$C_{m,unfold}$[b] (M urea)	$-m_{unfold}$[b] [kcal mol^{-1} (M urea)$^{-1}$]	$\Delta G_{unfold,app}^{H_2O}$[b] (kcal/mol)
1.44 μM WT TTR	3.14 ± 0.03	1.51 ± 0.10	4.7 ± 0.3
3.6 μM WT TTR	3.32 ± 0.02	2.29 ± 0.13	7.6 ± 0.4
7.2 μM WT TTR	3.42 ± 0.02	2.92 ± 0.25	10.0 ± 0.9
14.4 μM WT TTR	3.59 ± 0.01	3.49 ± 0.18	12.5 ± 0.7
36 μM WT TTR	3.77 ± 0.01	3.86 ± 0.20	14.6 ± 0.8
72 μM WT TTR	3.91 ± 0.01	3.89 ± 0.19	15.2 ± 0.7
144 μM WT TTR	4.05 ± 0.01	3.78 ± 0.19	15.3 ± 0.8
1.44−72 μM M-TTR[c]	3.07 ± 0.02 ($n = 7$)	1.50 ± 0.07 ($n = 7$)	4.61 ± 0.22 ($n = 7$)

[a] Apparent stabilities of WT TTR and M-TTR monomers were calculated from fitting of individual data sets at the indicated TTR concentration and are shown for a representative experiment (see Experimental Procedures for details). [b] Apparent values of $C_{m,unfold}$ and $-m_{unfold}$ were derived from fitting of the data shown in panels A and B of Figure 1 to eq 1, using the ratio of fluorescence intensities (F_{355}/F_{335}) as a measure of the extent of denaturation; $C_{m,unfold}$ is the urea concentration where TTR is 50% unfolded, and $-m_{unfold}$ is the urea dependence of the free energy of unfolding. Apparent values of $\Delta G_{unfold}^{H_2O}$ were determined by multiplying $C_{m,unfold}$ by $-m_{unfold}$. [c] Denaturation curves of M-TTR were identical at all concentrations that were examined (see Figure 1B for data and fits), and the values shown represent the mean and standard deviation of seven different data sets at varying M-TTR concentrations (1.44−72 μM).

Thermodynamic Stability of Monomeric TTR. Further evidence that the concentration dependence of monomer unfolding observed for WT TTR is due to the stability of the wild-type TTR tetramer is provided by control experiments carried out with M-TTR, an engineered monomeric variant of TTR that is >95% monomeric as purified and does not tetramerize under the conditions employed in these experiments, as determined by gel filtration and cross-linking studies (*19, 23*). Hence, urea denaturation of this variant involves only two species, the folded and unfolded monomers, and as expected, the denaturation curves show no dependence on M-TTR concentration (Figure 1B). Over a concentration range that varies more than 50-fold (1.44−72 μM), the M-TTR data are superimposable, allowing the direct determination of the tertiary structural stability of the M-TTR monomer from any one of the curves obtained. The $C_{m,unfold}$ for M-TTR is 3.07 ± 0.02 M urea, with an $-m_{unfold}$ of 1.50 ± 0.07 kcal mol^{-1} (M urea)$^{-1}$ ($n = 7$). Calculated values of $\Delta G_{unfold}^{H_2O}$ for denaturation curves at varying M-TTR concentrations are also indistinguishable, with an average of 4.61 ± 0.22 kcal/mol ($n = 7$). These values of $\Delta G_{unfold}^{H_2O}$ and $-m_{unfold}$ for M-TTR are close to those obtained for WT TTR at the lowest concentration that was examined (1.44 μM) and are in reasonable agreement with the previously reported stability parameters of M-TTR: $\Delta G_{unfold}^{H_2O}$ of 5.5 ± 0.8 kcal/mol and $-m_{unfold}$ of 1.7 ± 0.2 kcal mol^{-1} (M urea)$^{-1}$ (*19*). The small differences in measured stability may be due to slightly different experimental conditions used in the two studies. The thermodynamic parameters determined herein for M-TTR monomers are listed in Table 1, where they can be readily compared to the apparent stability of WT TTR monomers at varying TTR concentrations. For each of these parameters ($C_{m,unfold}$, $-m_{unfold}$, and $\Delta G_{unfold}^{H_2O}$), the apparent values determined from WT TTR experiments at 1.44 μM approach those calculated for M-TTR, suggesting that the tertiary structural stability of M-TTR is similar to that of WT TTR monomers.

Evaluating Quaternary Structural Changes in WT TTR. Although the described behavior for WT TTR monomer unfolding is that expected for a protein having linked quaternary and tertiary structural transitions at higher WT TTR concentrations, we also examined the tetramer−monomer equilibrium directly by two different methods, to verify that the two equilibria are indeed linked under these experimental conditions. Figure 2 shows the superposition of resveratrol binding data, monitoring the dissociation of WT TTR tetramers, with tryptophan fluorescence data, following tertiary structural changes, in a representative experiment utilizing 36 μM WT TTR. Independent fitting of each data set to a two-state denaturation model, corresponding either to the tetramer−monomer equilibrium in the case of the resveratrol binding data (fit to eq 2) or to the folded monomer−unfolded monomer equilibrium for the tryptophan fluorescence data (fit to eq 1), gave C_m values of 3.8 and 3.7 M urea for tetramer dissociation and monomer unfolding, respectively. The tetramer−monomer equilibrium as a function of urea concentration (36 μM WT TTR) was also assessed by chemical cross-linking quantified by densitometric analysis of the SDS−PAGE gel (Figure 3). As the concentration of urea is increased in these samples, the fraction of WT TTR present as tetramers (~55 kDa) decreases, with the concomitant appearance of a diffuse band corresponding to monomeric TTR (~14 kDa; the band becomes broad likely because several Lys residues are covalently modified with glutaraldehyde). Densitometry of the bands in each lane shows that dissociation proceeds from tetramer to monomer without any substantial accumulation of intermediates. The observed bands at ~42 and 28 kDa, which correspond to the molecular masses of trimeric and

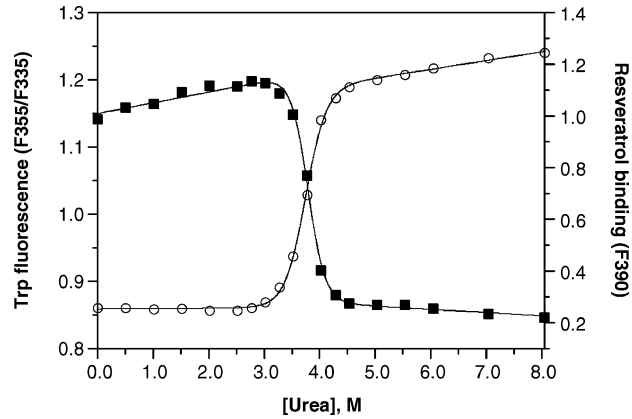

FIGURE 2: Urea denaturation of WT TTR. The denaturation of WT TTR (36 μM) was monitored both by intrinsic tryptophan fluorescence (○, left *y*-axis) to assess changes in the tertiary structure and by resveratrol binding (■, right *y*-axis) to assess tetramer dissociation. Samples were incubated for 96 h at 25 °C in the presence of varying concentrations of urea (0−8 M) prior to fluorescence measurements. Each data set was fit to a two-state denaturation model (eq 1 for tryptophan fluorescence data; eq 2 for resveratrol binding data) to give apparent C_m values of 3.8 and 3.7 M urea for tetramer dissociation and monomer unfolding, respectively.

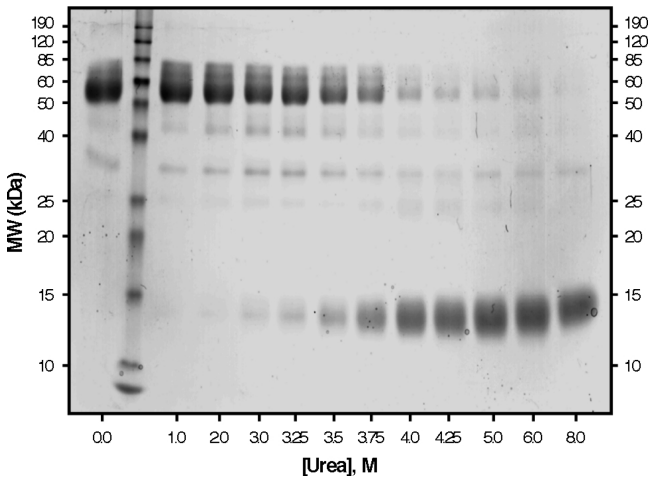

FIGURE 3: Chemical cross-linking of urea-denatured WT TTR. The same WT TTR samples (36 μM) analyzed by fluorescence in Figure 2 were also cross-linked with glutaraldehyde and analyzed by SDS−PAGE with Coomassie Blue staining (see Experimental Procedures for details). Molecular masses of protein standards (lane 2) are shown on the *y*-axis, and the urea concentration for each of the TTR samples is shown on the *x*-axis. The ~55 kDa bands correspond to TTR tetramers; these disappear as the concentration of urea is increased, with concomitant appearance of a diffuse monomer band at ~14 kDa. The bands observed at ~42 and 28 kDa probably correspond to trimeric and dimeric TTR, respectively. The intensity of each band was quantified by densitometry (not shown), and the $C_{m,diss}$ determined by this method was 3.7 or 3.8 M urea, depending on whether the percent tetramer or percent monomer data were used, in good agreement with the value determined by resveratrol binding (3.8 M; see Figure 2).

dimeric TTR, respectively, are present in all lanes and account for ~10% of the total TTR. A small increase in the intensity of these two bands (up to a maximum of ~18%) is apparent in lanes 4−7 (corresponding to 2.0−3.5 M urea, concentrations just below the $C_{m,diss}$ determined in this experiment), which indicates that these may be intermediate species in the dissociation of tetramers into monomers. Surprisingly, a small amount of tetrameric WT TTR (~5%) remains, even in the presence of 8 M urea, suggesting that a fraction of WT TTR tetramers is highly resistant to urea denaturation. Although we cannot rule out the possibility that this result may be due to a cross-linking artifact, it was only observed for WT TTR, with none of the other TTR variants displaying this behavior (vide infra). Fitting the densitometry data to eq 2 yielded a C_m for tetramer dissociation ($C_{m,diss}$) of 3.7 or 3.8 M urea, depending on whether the percent tetramer or percent monomer data were used, respectively, in excellent agreement with the value obtained above from resveratrol binding (3.8 M urea). As expected, $C_{m,diss}$ increases with an increase in TTR concentration and is nearly coincident with the $C_{m,unfold}$ values obtained at all the WT TTR concentrations examined [0.72−36 μM (data not shown)]. When considered together, these WT TTR data strongly support the conclusion that urea-induced tetramer dissociation and monomer unfolding of TTR occur simultaneously in these denaturation experiments, demonstrating that the equilibria are inextricably linked under these conditions. Since the concentrations of TTR used in these experiments represent the physiological concentration range of TTR (7.2−28.8 μM in plasma and 0.72−7.2 μM in CSF), it is reasonable to assume that tetramer dissociation and monomer unfolding equilibria are also thermodynamically linked in vivo.

Determining Quaternary and Tertiary Structural Stability Simultaneously from Concentration-Dependent WT TTR Denaturation Curves by Global Fitting. Due to the thermodynamic linkage of the WT TTR quaternary (tetramer dissociation) and tertiary (monomer unfolding) structural changes, we were unable to find conditions under which we could evaluate either equilibrium in a manner independent of the other. Therefore, we globally fit the concentration-dependent TTR urea denaturation data to a single set of parameters, allowing simultaneous quantification of quaternary and tertiary structural stability parameters. While a detailed explanation of the equations and methods used to determine WT TTR tetramer and monomer stabilities can be found in Experimental Procedures, the methodology is briefly discussed here. Because the two steps under investigation are thermodynamically linked, we assume there are three species (native tetramer, folded monomer, and unfolded monomer) that coexist in equilibrium, and the concentration of each species under a given set of conditions depends on the corresponding equilibrium constants, K_{diss} and K_{unfold} (Scheme 1; note that a model that accounted for only two species, native tetramer and unfolded monomer, gave a poor fit to the data, as shown in the Supporting Information). Starting with an equation for the total concentration of TTR (as the molar concentration of TTR monomers) that accounts for all three species, $[TTR_{total}] = 4[tetramer] + [monomer_{folded}] + [monomer_{unfolded}]$, and substituting in expressions for [tetramer] and $[monomer_{folded}]$ in terms of $[monomer_{unfolded}]$ and the two equilibrium constants, we obtain $[TTR_{total}] = 4([monomer_{unfolded}]^4/K_{diss}K_{unfold}^4) + ([monomer_{unfolded}]/K_{unfold}) + [monomer_{unfolded}]$ (see eq 3 in Experimental Procedures). This equation now relates the total TTR concentration, a known quantity, to the extent of monomer unfolding, which can be determined experimentally from the tryptophan fluorescence measurements, and the two unknowns of interest, K_{diss} and K_{unfold}. The values of K_{diss} and K_{unfold} are related to the free energies of tetramer dissociation (ΔG_{diss}) and unfolding (ΔG_{unfold}), respectively, which are in turn linearly related to the urea concentration with slopes $-m_{diss}$ and $-m_{unfold}$, respectively; this relationship is summarized by eq 3 in Experimental Procedures. The values of ΔG_{diss}, ΔG_{unfold}, $-m_{diss}$, and $-m_{unfold}$ can now be estimated if the extent of monomer unfolding is determined over a range of TTR concentrations, and the resulting data are analyzed globally by fitting them to eq 3.

The power of this method is that we can, for the first time, assess the true stability of TTR tetramers and monomers, as long as other intermediates (e.g., dimers or trimers) are not extensively populated. The free energies determined by this analysis for tetramer dissociation and monomer unfolding are actual, rather than apparent, stability values determined under specified conditions and useful for comparisons among variants under the same conditions. Hence, the stability of WT TTR and various disease-associated variants can be compared and integrated with known dissociation and unfolding rates (*7, 8, 12, 13, 18, 47*), to gain insight into factors that may lead to amyloid disease. Another advantage of the method is that stability parameters can be derived using only tryptophan fluorescence data. This advantage is significant not only because of the ready availability and

Table 2: Comparison of Thermodynamic Stabilities of TTR Tetramers and Monomers[a]

	tetramers		monomers	
	$\Delta G_{diss}^{H_2O}$ (kcal/mol)	$-m_{diss}$ [kcal mol^{-1} (M urea)$^{-1}$]	$\Delta G_{unfold}^{H_2O}$ (kcal/mol)	$-m_{unfold}$ [kcal mol^{-1} (M urea)$^{-1}$]
WT	32.8 ± 2.2	2.7 ± 0.1	4.0 ± 0.5	1.4 ± 0.1
V122I	25.6 ± 1.0	1.5 ± 0.4	5.1 ± 0.2	1.6 ± 0.1
L55P	33 ± 7	2.8 ± 0.4	2.0 ± 1.5	1.6 ± 0.5
V30M	nd[b]	nd[b]	nd[b]	nd[b]
A25T	nd[c]	nd[c]	nd[c]	nd[c]

[a] Thermodynamic stabilities were calculated by global analysis of concentration-dependent denaturation data, as described in Experimental Procedures. The stability of TTR tetramers is described by $\Delta G_{diss}^{H_2O}$, the free energy of tetramer dissociation in the absence of denaturant, and $-m_{diss}$, the dependence of ΔG_{diss} on urea concentration. TTR monomer stability is described by $\Delta G_{unfold}^{H_2O}$, the free energy of monomer unfolding in the absence of denaturant, and $-m_{unfold}$, the urea dependence of ΔG_{unfold}. [b] Thermodynamic stabilities could not be calculated by global fitting because urea denaturation curves did not fit a two-state model (see Figures 4C, 5C, and 6). [c] Thermodynamic stabilities could not be calculated by global fitting due to aggregation of A25T at low urea concentrations (see Figures 4D and 5D).

simplicity of fluorescence spectroscopy but also because intrinsic protein fluorescence does not perturb the equilibrium when the extent of denaturation is being assessed. In contrast, both methods used previously to measure tetramer quaternary structural stability (resveratrol binding and chemical cross-linking) have the potential to shift the tetramer−monomer equilibrium. Globally fitting the concentration-dependent urea denaturation data obviates our dependence on these techniques for measuring tetramer concentrations as a function of TTR and urea concentrations.

As described in full detail in Experimental Procedures, global analysis of concentration-dependent TTR denaturation data yields information about the thermodynamics of dissociation, expressed as $\Delta G_{diss}^{H_2O}$ and $-m_{diss}$, and the thermodynamics of unfolding, expressed as $\Delta G_{unfold}^{H_2O}$ and $-m_{unfold}$. The results of this fluorescence analysis for the tetrameric TTR variants that conform to the two-step denaturation model (WT TTR, V122I, and to a lesser extent L55P) are discussed in turn in the following paragraphs, and the corresponding data are summarized in Table 2. Other variants (V30M and A25T) that do not conform to this model are then discussed in more qualitative terms.

WT TTR Tetramer and Monomer Thermodynamic Stability Determined by Global Fitting. Global fitting of the concentration-dependent fluorescence-based denaturation data affords the following WT TTR stability parameters: $\Delta G_{diss}^{H_2O}$ = 32.8 ± 2.2 kcal/mol, and $-m_{diss}$ = 2.7 ± 0.1 kcal mol^{-1} (M urea)$^{-1}$; $\Delta G_{unfold}^{H_2O}$ = 4.0 ± 0.5 kcal/mol, and $-m_{unfold}$ = 1.4 ± 0.1 kcal mol^{-1} (M urea)$^{-1}$. The global fit to the denaturation data is shown in the Supporting Information. The thermodynamic stability of the WT TTR monomer determined by global analysis is lower than that of M-TTR by ~0.6 kcal/mol (*19*), probably because of the two Met mutations in the latter sequence (F87M and L110M). Although the nearly superimposable denaturation curves obtained for M-TTR and 1.44 μM WT TTR seem to indicate that the stabilities of the monomers of WT TTR and M-TTR are very similar, it is clear from the results presented above that WT TTR monomer unfolding is still thermodynamically linked to tetramer dissociation, even at the lowest WT TTR concentration examined here. Hence, the true tertiary structural stability of WT TTR must be lower than the $\Delta G_{unfold,app}^{H_2O}$ for denaturation of 1.44 μM WT TTR (4.7 kcal/mol), and the value of $\Delta G_{unfold}^{H_2O}$ of 4.0 kcal/mol obtained for WT TTR by global fitting is reasonable.

We had previously noted that the WT TTR quaternary and tertiary structural equilibria appear to become partially unlinked when the WT TTR concentration is decreased to ≤0.72 μM, and it is useful to reexamine how low a concentration of WT TTR would be needed to completely unlink these equilibria. The ΔG_{diss} calculated here, 32.8 kcal/mol, corresponds to a dissocation constant, K_{diss}, of 9 × 10^{-25} M^3. The magnitude of this tetramer dissociation constant means that even at a concentration of 0.72 μM, WT TTR is >95% tetrameric in the absence of urea. Furthermore, if we assume that >90% dissociation of the tetramer to monomers (fraction tetramer, α = 0.10) would be required to completely unlink the two equilibria, then we can estimate that unlinking would only be accomplished at WT TTR concentrations of <3.6 nM, much lower than what is attainable in these experiments.

Having calculated the thermodynamic parameters for WT TTR by globally fitting the data, we can now do the same for the TTR disease-associated variants and comment on the extent of thermodynamic linkage exhibited by their quaternary and tertiary structural transitions. We can also determine whether the mechanism of denaturation and unfolding of WT TTR applies to the mutant disease-associated TTR sequences.

V122I TTR Forms a Destabilized Tetramer and a Stable Monomer. The V122I mutation is examined first because it affects more people than any other TTR mutation; only WT TTR deposition in senile systemic amyloidosis is clinically more significant. Figure 4A shows representative concentration-dependent V122I denaturation curves monitored by tryptophan fluorescence. The individual denaturation curves fit well to eq 1, revealing C_m values ranging from ~3.3 to ~3.8 M urea, and $-m_{unfold}$ values ranging from ~1.5 to ~3.3 kcal mol^{-1} (M urea)$^{-1}$. Notably, the apparent value of each parameter increases gradually as the V122I concentration is increased from 1.44 to 144 μM; however, the denaturation curves appear to be much closer together, especially for the first three curves (corresponding to concentrations of 1.44, 3.6, and 7.2 μM), than those observed with WT TTR, indicating the defect with V122I may be in tetramer stability.

Global analysis of the concentration-dependent data (see the Supporting Information) confirms that the quaternary structure of V122I is destabilized, as reflected in the thermodynamic parameters determined for V122I tetramers: $\Delta G_{diss}^{H_2O}$ = 25.6 ± 1.0 kcal/mol, and $-m_{diss}$ = 1.5 ± 0.4 kcal mol^{-1} (M urea)$^{-1}$. This destabilization of the tetramer, ~7 kcal/mol relative to WT TTR, translates into a dissociation constant for tetramerization that is 6 orders of magnitude larger for V122I than for WT TTR (10^{-18} and 10^{-24} M^3, respectively).

From the global fitting results, it appears that the tertiary structural stability of V122I ($\Delta G_{unfold}^{H_2O}$) equals 5.1 ± 0.2

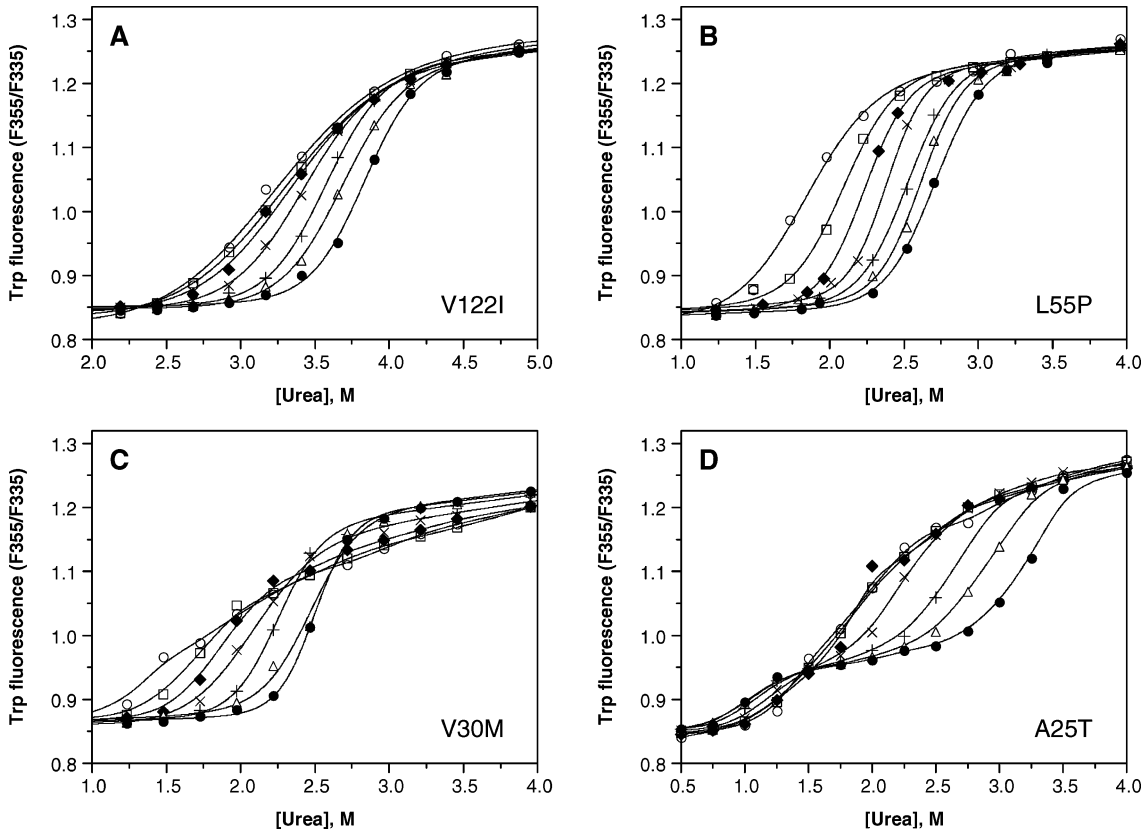

FIGURE 4: Dependence of urea denaturation of V122I (A), L55P (B), V30M (C), and A25T TTR (D) on protein concentration. Denaturation reaction mixtures contained TTR (1.44−144 μM) and were incubated for 96 h at 4 °C in the presence of varying concentrations of urea (0−8 M) prior to fluorescence measurements (see Experimental Procedures for details). TTR concentrations for each variant were 1.44 (○), 3.6 (□), 7.2 (◆), 14.4 (×), 36 (+), 72 (△), and 144 μM (●). The denaturation curves of V122I (A) and L55P (B) resemble those observed for WT TTR (see Figure 1A), with the steepness of the transition slope increasing and the curves shifting progressively further to the right with an increase in the TTR concentration. In contrast, for the remaining variants, V30M (C) and A25T (D), two transitions are observed in each curve, and the data cannot be fit to a two-state denaturation model (solid lines shown in these panels represent smoothing curves, rather than fits of the data to eq 1). Nevertheless, for all of the variants, the apparent stability of TTR to urea denaturation increases with an increase in the TTR concentration (C_m increases from 3.3 to 3.8 M urea for V122I, from 1.9 to 2.8 M urea for L55P, from 1.5 to 2.5 M urea for V30M, and from 1.7 to 3.1 M urea for the second transition of A25T; note that the panels have different *x*-axis scales).

kcal/mol with an $-m_{unfold}$ of 1.6 ± 0.1 kcal mol^{-1} (M urea)$^{-1}$. These results indicate that V122I monomers are more stable than those of WT TTR, by 1.1 ± 0.5 kcal/mol. However, the previously reported stability of M-V122I is ∼0.8 kcal/mol lower than that of M-TTR, with a $\Delta G_{unfold}^{H_2O}$ of 4.7 ± 0.2 kcal/mol and an $-m_{unfold}$ of 1.4 ± 0.1 kcal mol^{-1} (M urea)$^{-1}$ (*9*); compare these values to a $\Delta G_{unfold}^{H_2O}$ for M-TTR of 5.5 ± 0.8 kcal/mol under the same conditions (*19*). Again, this discrepancy is likely attributable to the F87M and L110M mutations in M-TTR constructs and the differences in the denaturation conditions used in this and previous work.

The effects of the V122I mutation on tetramer stability (less stable than WT TTR) and monomer stability (possibly slightly more stable than WT TTR) offset each other to some extent, accounting for our previous conclusion that V122I and WT TTR have similar overall thermodynamic stabilities (*7*). However, this offsetting is not perfect, and there are significant differences between the two proteins at equilibrium. In particular, at physiological concentrations ([TTR_{total}] = 14.4 μM), the amount of unfolded monomer for V122I TTR (0.15 nM) is 3-fold higher than for WT TTR (0.05 nM). Although these concentrations of unfolded monomer are low, this thermodynamic difference, combined with the rate of dissociation being 2-fold faster than that of WT ($t_{1/2}$ = 19 h vs 41 h for WT TTR) (*7*), likely contributes to the relatively early development of V122I cardiomyopathy.

Chemical cross-linking of V122I TTR (36 μM) in increasing urea concentrations shows that dissociation of tetramers of this variant proceeds completely to monomers without a significant accumulation of intermediates (Figure 5A). Fitting the densitometry data with eq 2 gives a $C_{m,diss}$ of 3.5 M (from percent tetramer data) or 3.6 M urea (from percent monomer data). This value is in good agreement with the $C_{m,diss}$ determined from resveratrol binding (3.4 M urea), and with the C_m determined from tryptophan fluorescence (3.6 M urea) for these same samples (data not shown).

L55P Exhibits a Complex Denaturation Pathway. L55P is a rare but extremely pathogenic mutation in TTR, associated with amyloidosis in the second to third decade of life (the earliest onset amyloid disease known) (*48*). Urea denaturation curves for L55P obtained by intrinsic tryptophan fluorescence over a range of L55P concentrations are shown in Figure 4B. Although the apparent values of $C_{m,unfold}$ are lower than those obtained for WT TTR at each TTR concentration examined, the pattern of behavior is similar to that observed for WT TTR, namely, that each denaturation curve fits nicely to a two-state denaturation model and that L55P TTR appears to become more stable (curves shifting

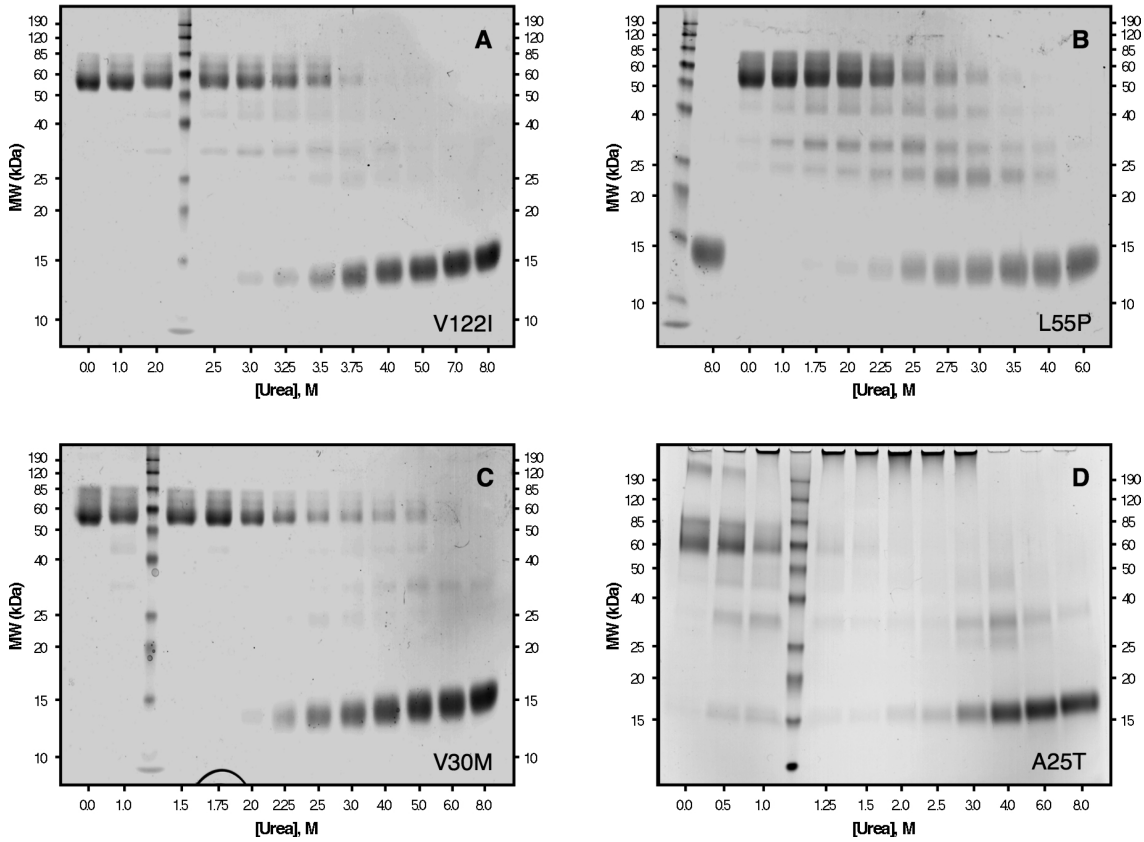

FIGURE 5: Chemical cross-linking of urea-denatured V122I (A), L55P (B), V30M (C), and A25T (D). TTR samples (36 μM for panels A−C and 144 μM for panel D) were cross-linked with glutaraldehyde and analyzed by SDS−PAGE with Coomassie Blue staining (see Experimental Procedures for details). Molecular masses of protein standards are shown on the *y*-axis, and the urea concentration for each of the TTR samples is shown on the *x*-axis. The bands at ~55 kDa correspond to TTR tetramers; these disappear as the concentration of urea is increased, with the concomitant appearance of a diffuse monomer band at ~14 kDa. The denaturations of V122I (A) and V30M (C) resemble the data obtained for WT TTR (see Figure 3), in that for these three variants, the main species observed are the native tetramer and the denatured monomer (although some trimer and dimer are observed for V30M TTR). In contrast, when L55P is denatured (B), a significant fraction of dimeric TTR species (seen as bands at ~28 and ~23 kDa) accumulates at intermediate urea concentrations. For the A25T variant (D), aggregation is observed rather than denaturation at low urea concentrations. The aggregates formed are large, do not enter the gel, and accumulate maximally around 2.0 M urea. Higher concentrations of urea denature the aggregates into monomers.

to higher urea concentrations and to steeper transition regions) as the L55P concentration increases. Fitting the individual denaturation curves with eq 1 gives apparent values of $C_{m,unfold}$ increasing from ~1.9 to ~2.8 M urea and of $-m_{unfold}$ increasing from ~2.5 to ~3.5 kcal mol^{-1} (M urea)$^{-1}$ as the concentration of L55P is increased from 1.44 to 144 μM.

Global analysis of the concentration-dependent data affords the following thermodynamic parameters for L55P (see the Supporting Information): $\Delta G_{diss}^{H_2O} = 33 \pm 7$ kcal/mol, and $-m_{diss} = 2.8 \pm 0.4$ kcal mol^{-1} (M urea)$^{-1}$; $\Delta G_{unfold}^{H_2O} = 2.0 \pm 1.5$ kcal/mol, and $-m_{unfold} = 1.6 \pm 0.5$ kcal mol^{-1} (M urea)$^{-1}$. The value of $\Delta G_{diss}^{H_2O}$ for L55P TTR derived from the fit is similar to that of WT TTR, even though a plethora of other data suggests that the L55P tetramer is less stable [e.g., the dissociation rate of the L55P tetramer is ~9-fold faster than that of the WT TTR tetramer (*7*), and L55P TTR tetramers dissociate at higher pH values than WT TTR tetramers (*10, 42*)]. These observations and the large error in the parameter estimates from the global fit raise the suspicion that the two-step model used in the global analysis does not describe the denaturation pathway of L55P TTR well. Consistent with this supposition, chemical cross-linking of the same samples reveals several intermediate species (Figure 5B). Three different bands, with apparent molecular masses of 42, 28, and 23 kDa, are observed as the tetramer dissociates. These bands are likely attributable to trimeric and dimeric TTR, respectively, and appear to be intermediates in the denaturation of L55P TTR.

The effect of the complicated denaturation mechanism of L55P TTR on the parameter estimates derived from our global fit is difficult to predict in detail but should affect tetramer stability more than monomer stability. Consistent with this notion, the difference between the values of $\Delta G_{unfold}^{H_2O}$ for L55P (2.0 kcal/mol) and WT TTR (4.0 kcal/mol) is 2.0 kcal/mol, consistent with previous experiments with the engineered monomeric version of L55P (M-L55P, with L55P, F87M, and L110M mutations), which also exhibits a destabilization of ~2 kcal/mol relative to M-TTR (F87M and L110M mutations only). M-L55P affords a $\Delta G_{unfold}^{H_2O}$ of 3.3 ± 0.1 kcal/mol and an $-m_{unfold}$ of 1.9 ± 0.1 kcal mol^{-1} (M urea)$^{-1}$ (X. Jiang, P. Hammerström, and J. W. Kelly, unpublished results) compared to the $\Delta G_{unfold}^{H_2O}$ for M-TTR of 5.5 ± 0.8 kcal/mol under the same conditions (*19*).

V30M TTR Denaturation Cannot Be Fit to a Two-State Model. The V30M mutation in TTR, which leads to the vast majority of FAP cases, is second in clinical importance among the disease-associated TTR mutations (*3*). Urea denaturation curves for V30M TTR are shown in Figure 4C,

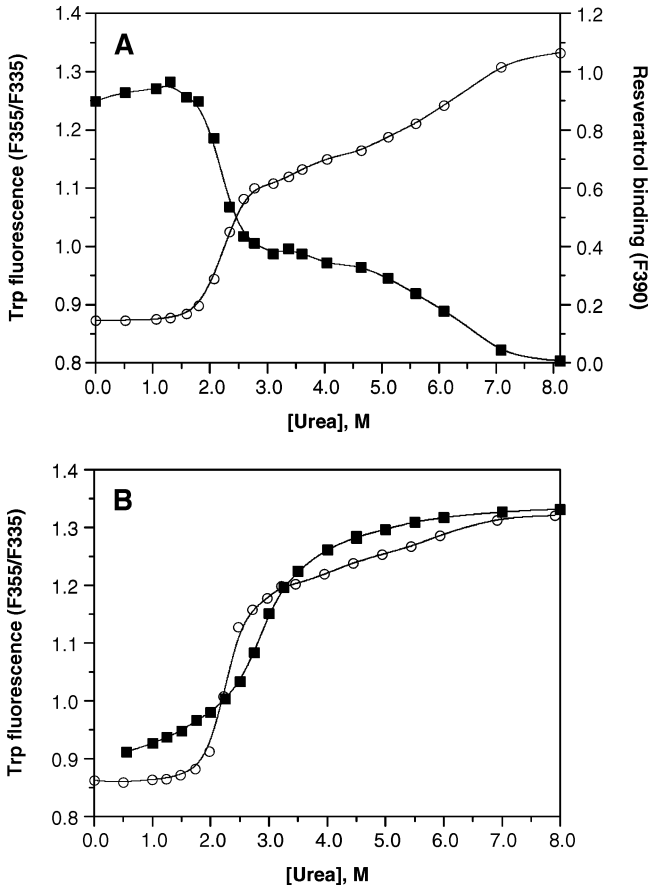

FIGURE 6: Urea denaturation of V30M. (A) The denaturation of V30M (36 μM) was monitored both by intrinsic tryptophan fluorescence (○, left *y*-axis) to assess changes in the tertiary structure and by resveratrol binding (■, right *y*-axis) to assess tetramer dissociation. Samples were incubated for 96 h at 25 °C in the presence of varying concentrations of urea (0−8 M) prior to fluorescence measurements. Using either method, two transitions can be clearly seen in the denaturation curves, and the data cannot be fit to a two-state denaturation model. (B) Curves for the denaturation (○) and renaturation (■) of V30M (36 μM), assessed by intrinsic tryptophan fluorescence, are compared. For the denaturation experiment, samples were incubated for 96 h at 4 °C in the presence of varying concentrations of urea (0−8 M); note that the lower temperature used here minimizes but does not eliminate the second transition (compare with panel A). For the renaturation experiment, V30M (520 μM) was completely denatured by incubating the sample for 96 h at 4 °C in 8 M urea. The denatured V30M was subsequently diluted into renaturation reaction mixtures containing varying concentrations of urea (0.55−8 M), and the samples were incubated for 24 h at 25 °C prior to fluorescence measurements. The second transition observed in the denaturation curve is absent in the renaturation curve; however, V30M cannot be completely refolded under these conditions, and furthermore, the two curves do not overlap in the transition region. Solid lines in both panels represent smoothing curves of the data.

carried out over a V30M TTR concentration range of 1.44−144 μM. The curves shift to the right with an increase in V30M concentration, giving apparent C_m values for denaturation (estimated visually from the graph) that increase from ~1.5 M urea at 1.44 μM V30M to ~2.5 M urea at 144 μM V30M. However, examination of any of the individual data sets obtained for this mutant reveals an unusual shape (this is best seen in Figure 6A for data obtained in a separate experiment at a V30M concentration of 36 μM). Fitting the concentration-dependent denaturation curves to eq 1 gives poor fits in all cases, yielding a small amplitude for the transition region and an apparently very steep post-transition slope, with the data points in this region deviating significantly and in a nonrandom manner from the fit. In fact, each individual curve appears to display two transition regions, both of which vary with the concentration of V30M. When denaturation curves derived from Trp fluorescence measurements are plotted with resveratrol binding data obtained in parallel [36 μM V30M, incubation for 96 h at 25 °C instead of 4 °C (Figure 6A)], the two transition regions observed in each curve are symmetrical and exactly coincident, with apparent C_m values estimated to be ~2.2 and 6.5 M urea.

The same samples were also examined by glutaraldehyde cross-linking using SDS−PAGE quantification by densitometry (Figure 5C). Like those of WT TTR, the cross-linking data reveal a small accumulation of trimeric and dimeric V30M quaternary structures between 3.0 and 6.0 M urea (Figure 5C, lanes 8−11), although with V30M TTR this accumulation occurs between the two transition regions observed by Trp fluorescence whereas with WT TTR it occurs before the single transition. Resveratrol binding is weakly dependent on urea concentration in this range, suggesting that V30M TTR dissociation intermediates may be able to bind resveratrol. Such a dissociation pathway would be in stark contrast to that of WT TTR, which dissociates into dimers that do not contain a small molecule binding site (*16, 49*).

V30M is kinetically stable relative to WT TTR (*7*), consistent with a more robust small-molecule-binding dimer interface. The possibility that a slow rate of tetramer dissociation ($t_{1/2}$ = 68 h, compared with 41 h for WT TTR) might be responsible for the biphasic denaturation curves was examined. The samples were incubated for varying lengths of time (24−334 h rather than the usual 96 h), and the extent of denaturation at each time point was measured by Trp fluorescence. Although longer incubation times do increase the amplitude of the first transition and decrease the amplitude of the second transition, both transitions are still apparent, even after incubation for two weeks [t = 334 h (data not shown)]. Fitting the time-dependent fluorescence changes at each urea concentration to single exponentials indicates that, while the rates of approach to equilibrium increase nonlinearly with urea concentration, as previously reported (*7*), equilibrium should be reached in all cases at $t \leq 334$ h (data not shown). Since the two transitions are still apparent at this time point, where no further changes in the fluorescence signal are observed, there may be a thermodynamic as well as a kinetic explanation for the observed phenomenon, i.e., the stabilization of a TTR dimer that is not populated during WT TTR denaturation. The amplitude of the second transition is smaller at lower incubation temperatures [compare the tryptophan fluorescence denaturation data in panels A (25 °C) and B (4 °C) of Figure 6], presumably because TTR dissociation is faster at lower temperatures (*47*), but it is still present. While the second transition could be minimized, it could not be eliminated when equilibrium is approached by denaturing the tetramer.

To gain further insight into the complex behavior exhibited by V30M TTR, renaturation was studied by diluting a V30M solution completely denatured in the presence of 8 M urea (complete within 96 h). Samples diluted to a final urea concentration of 0.55−8.0 M were incubated for an additional 24 h (25 °C) and studied by Trp fluorescence.

Although the second transition was absent in this renaturation experiment, and the post-transition region (4.0−8.0 M urea) appeared to be more typical, V30M did not completely refold at low urea concentrations (Figure 6B), suggesting significant kinetic barriers in both directions, especially at intermediate urea concentrations. Furthermore, the poor overlap of the two data sets in the transition region is evidence that denaturation and renaturation are not fully reversible for this variant. Increasing the incubation time in the renaturation experiment had no effect on the data (not shown). In contrast to these observations, coincident denaturation and renaturation curves are observed for WT TTR and several other TTR variants (L55P, V122I, and M-TTR), demonstrating that equilibrium is reached regardless of whether it is approached in a denaturation or renaturation direction (data not shown).

Although V30M is clearly less stable than WT TTR, as evidenced by its much lower C_m for denaturation (C_m of ~1.5 M urea for V30M vs ~3.1 M urea for WT TTR at 1.44 μM), its peculiar behavior under both denaturation and renaturation conditions precludes quantification of its thermodynamic parameters. Previous denaturation studies reveal that M-V30M is destabilized by ~2.5 kcal/mol relative to M-TTR, with a $\Delta G_{unfold}^{H_2O}$ of 3.0 ± 0.2 kcal/mol and an $-m_{unfold}$ of 2.0 ± 0.1 kcal mol^{-1} (M urea)$^{-1}$ (X. Jiang, P. Hammerström, and J. W. Kelly, unpublished results); compare those to a $\Delta G_{unfold}^{H_2O}$ for M-TTR of 5.5 ± 0.8 kcal/mol under the same conditions (*19*). Furthermore, the magnitude of the shift in C_m values (to ~1 M higher urea) observed when the V30M concentration is increased 100-fold, from 1.44 to 144 μM, is similar to the shift observed for WT TTR (to ~0.9 M higher urea) over the same concentration range, perhaps reflecting a similar quaternary structural stability, albeit one with a distinct mechanism of dissociation. Thus, it appears likely that V30M TTR tetramers are at least as stable as those of WT TTR but have an unusual dissociation mechanism and a destabilized tertiary structure, with the latter two effects conspiring to predispose individuals with this mutation to TTR amyloidogenesis. The kinetic stability of the V30M tetramer probably protects carriers of V30M against a more severe FAP pathology (*7*).

A25T Is Highly Destabilized and Prone to Aggregation. Urea denaturation of A25T shows that this TTR variant behaves unlike any of the others that were examined. The concentration-dependent tryptophan fluorescence curves for A25T TTR are shown in Figure 4D. Denaturation curves obtained at low A25T TTR concentrations (0.72−7.2 μM) appear to fit well to eq 1, but unlike what is observed with the other variants, there is virtually no concentration dependence of the fitting parameters, with values of C_m of ~1.7 M urea and $-m_{unfold}$ of ~1.3 kcal mol^{-1} (M urea)$^{-1}$ obtained for each curve in this concentration range (0.72 μM curve not shown). As the A25T TTR concentration is increased further (from 7.2 to 144 μM), the characteristic shifting of the curves to the right and an increased steepness of the transition region are observed. The most striking feature of these denaturation curves, however, is the appearance of a unique second transition region at A25T TTR concentrations greater than 7.2 μM. The C_m for this second transition, visually estimated from Figure 4D, increases from ~1.7 M urea at 7.2 μM A25T TTR to ~3.1 M urea at 144 μM A25T TTR. The shapes of the curves superficially resemble those of V30M TTR, but the nature and origin of the additional transition are clearly different.

The first indication that these data were unusual came from direct observation of the fluorescence spectra collected at low urea concentrations, where dramatic increases in the fluorescence intensity at each of the wavelengths examined (335 and 355 nm) were apparent, even when the fluorescence ratio (F_{355}/F_{335}) was not changing appreciably (data not shown). The effect was greater for samples containing higher concentrations of A25T TTR. The samples were slightly cloudy to the eye, and turbidity measurements showed a corresponding increase in turbidity in this same region of the denaturation curves (data not shown), suggesting that aggregation of A25T TTR occurs under these conditions. Additional direct evidence for aggregation was obtained by cross-linking followed by SDS−PAGE, which clearly shows the appearance of very large aggregates of A25T at low urea concentrations (Figure 5D). In the 144 μM samples shown here (where aggregation is most favored), the aggregates accumulate maximally at 2.0 M urea (lane 7), where they represent nearly 85% of the total A25T TTR in the sample. These large aggregates are apparently disrupted at higher concentrations of urea (>4.0 M; lanes 10−12), yielding monomeric A25T TTR as the predominant species. Trimeric (molecular mass of ~42 kDa) and dimeric (molecular mass of ~28 kDa) species are observed as intermediates in both the aggregation and disaggregation of A25T TTR, accumulating to a maximum of ~30% at 1.0 M urea (aggregation phase) and ~32% at 4.0 M urea (disaggregation phase). A25T TTR apparently aggregates in the absence of any denaturation stress, as evidenced by the presence of a species with a molecular mass of >190 kDa (~15% of total A25T) and the very large aggregates that do not enter the gel (~5% of A25T), in the 0 M urea sample (lane 1).

Fitting the densitometry data for the disappearance of A25T TTR tetramers and the appearance of A25T TTR monomers to eq 2 gives C_m values of 1.2 and 3.1 M urea, respectively. The two transitions are coincident with the appearance (C_m = 1.2 M urea) and disappearance (C_m = 3.1 M urea) of the aggregates (data not shown). These observations suggest that the first transition in the fluorescence data corresponds to the aggregation of A25T TTR (presumably preceded by tetramer dissociation and partial denaturation of the monomers), and the second transition is the disaggregation of the large aggregates, resulting in unfolded monomers. At low A25T TTR concentrations, the methods employed do not detect aggregates, which presumably would form to a lesser extent at low protein concentration, and the denaturation curves monitored by tryptophan fluorescence show a single transition.

Because A25T clearly does not undergo a tetramer-folded monomer−unfolded monomer denaturation process, the data cannot be fit by global analysis to yield thermodynamic parameters. However, fitting the individual denaturation curves at low A25T TTR concentrations (where aggregation is not observed) to eq 1 gives us an upper limit on the stability of the A25T TTR monomer. The apparent tertiary structural stability, given by a $\Delta G_{unfold}^{H_2O}$ of 1.8 ± 0.2 kcal/mol and an $-m_{unfold}$ of 1.1 ± 0.0 kcal mol^{-1} (M urea)$^{-1}$ (n = 3), is lower than the previously reported $\Delta G_{unfold}^{H_2O}$ of 2.8 kcal/mol (*12*). Although the calculated $\Delta G_{unfold}^{H_2O}$ represents an apparent stability value, it may in fact closely

approximate the true monomeric stability of this variant, since the overlapping curves over a 10-fold A25T concentration range (0.72−7.2 μM) suggest that tetramer dissociation and monomer unfolding are not appreciably linked at low concentrations. The observation that the equilibria are at least partially unlinked at A25T concentrations as high as 7.2 μM indicates that the tetrameric structure is probably highly destabilized as well, consistent with the disappearance of tetramer at urea concentrations lower than those of any of the other TTR variants studied herein (see Figures 3 and 5).

In summary, the thermodynamic stability profile of A25T shows that both tetramers and monomers of this variant are highly destabilized. In addition, the rate of A25T TTR tetramer dissociation is extremely fast, with a $t_{1/2}$ of ~2.1 min (~1200-fold faster than the dissociation of WT TTR) (*12*), reflecting a high degree of kinetic destabilization of the quaternary structure. These factors together probably contribute to the high propensity of A25T to aggregate in vitro (*12, 13*). Paradoxically, the extreme instability of A25T appears to be protective against aggressive systemic amyloid disease, in that the serum concentrations of variant protein are very low due to extensive ERAD by cellular quality control during secretion. ERAD occurs to a greater extent in the liver than in the choroid plexus, partially explaining the CNS phenotype of this amyloid disease (*12, 13*). That this is one of the few disease-associated TTR variants that is substantially degraded by the cellular secretory pathway supports the fact the quaternary and tertiary structural stability of A25T are significantly compromised.

CONCLUDING REMARKS

Our results are broadly consistent with previous findings on the stabilities of TTR variants (*7–15, 17, 18, 22, 42*). However, the concentration-dependent denaturation data obtained herein and the global fits to these data (where possible) add substantial detail. Combining our data with that available in the literature yields the following picture of TTR stability and the effect of mutations thereon. WT and V122I TTR both have simple denaturation pathways (tetramer−folded monomer−unfolded monomer) and stable monomers, but the WT forms more stable tetramers than V122I. V30M and L55P TTR both have complicated denaturation pathways and unstable monomers, but V30M tetramers are quite stable (possibly even more so than WT tetramers). L55P tetramers are less stable than V30M tetramers but are still sufficiently stable to be the dominant species at physiological TTR concentrations. Finally, A25T TTR has unstable monomers, dramatically destabilized tetramers, and a complicated denaturation pathway that includes substantial amounts of aggregate formation, unstable monomers, and dramatically destabilized tetramers.

Categorizing the TTR variants studied herein according to the phenotypes of their associated amyloid diseases reveals groupings that are strikingly similar to those described above. WT TTR and V122I TTR are associated with late onset cardiac amyloid diseases, with the latter being more aggressive than the former (*29*). V30M TTR and L55P TTR are associated with early onset polyneuropathy, again with the latter being more aggressive than the former (*48*). Finally, A25T TTR is not associated with systemic amyloidosis, because it is extensively degraded in liver cells by ERAD (*12, 13*). Rather, the high concentration of thyroxine in the choroid plexus stabilizes A25T TTR enough for it to be secreted into the central nervous system where it appears to cause central nervous system selective amyloidosis after dissociation of thyroxine in the CSF (*12, 13*).

The correspondence between the thermodynamic and amyloidosis phenotype groupings of the TTR variants suggests a relationship between TTR folding and tetramerization energetics and disease pathology. TTR variants with unstable monomers and complex tetramer dissociation pathways (V30M and L55P TTR; A25T is discussed separately below) appear to cause early onset TTR amyloid diseases. In contrast, TTR variants with stable monomers and straightforward tetramer dissociation pathways (WT and V122I TTR) appear to cause TTR amyloid diseases with a substantially later onset. Thus, monomer instability and/or complicated tetramer dissociation pathways, both of which should increase the rate of partitioning of TTR into aggregation pathways (*50*), seem to be a primary source of TTR pathogenicity. Tetramer stability also affects TTR pathogenicity but in a more complicated way. Moderate decreases in tetramer stability appear to shift the age of onset of TTR amyloid disease. For example, V122I TTR amyloidosis occurs earlier than WT TTR amyloidosis and L55P TTR amyloidosis occurs earlier than V30M TTR amyloidosis. This effect, however, is secondary to the effect of monomer instability and complicated dissociation pathways, as V122I TTR amyloidosis occurs substantially later than V30M TTR amyloidosis. As tetramer instability becomes extreme, TTR variants with unstable monomers like A25T TTR become susceptible to ERAD and do not cause systemic amyloid disease (*8, 12, 13, 41*). Notably, the stabilities of V30M and L55P TTR monomers are approximately the same as those of several monomeric TTR variants that have been shown to undergo extensive ERAD (*13*). It seems that for V30M and L55P TTR, tetramerization stabilizes the proteins enough to "chaperone" them out of the ER and through the export pathway.

Finally, the relationship between TTR stability and pathology presented above provides insight into therapeutic strategies for TTR amyloidosis. On the basis of the discussion given above, the small molecule binding strategy for treating TTR amyloidosis described in the introductory section would be only marginally beneficial if small molecule binding did nothing more than stabilize TTR tetramers; as noted above, tetramer stabilization appears to have a secondary role in TTR amyloidosis. Tetramer dissociation kinetics, however, trump the effects of tetramer stability, monomer stability, and complicated dissociation pathways. This assertion is supported by the observation mentioned in the introductory section that T119M TTR subunits, which slow the dissociation of TTR tetramers into which they have been incorporated, can ameliorate TTR amyloidosis in T119M/V30M TTR compound heterozygotes (*17, 18, 35*). Fortunately, small molecule binding greatly slows tetramer dissociation by imparting kinetic stabilization (*18, 20, 21*), increasing the likelihood that this therapeutic strategy will be effective. Clinical trials for small molecule kinetic stabilizer treatment of TTR amyloidosis are now underway and will soon inform us if the relationship between TTR energetics and TTR amyloid disease phenotype proposed above is correct.

ACKNOWLEDGMENT

We thank Maria Dendle and Michael Saure for their help with protein expression and Nora Green for providing A25T TTR. We also thank Per Hammarström and R. Luke Wiseman for critically reading the manuscript and Natàlia Reixach and members of the Kelly laboratory for helpful discussions.

SUPPORTING INFORMATION AVAILABLE

A plot showing the relatively poor global fit to a two-state model (native tetramer and unfolded monomer) for WT TTR and plots showing the global fit of our three-state model (native tetramer, folded monomer, and unfolded monomer) to the concentration-dependent urea denaturation data for WT, V122I, and L55P TTR. This material is available free of charge via the Internet at http://pubs.acs.org.

REFERENCES

1. Kelly, J. W. (1998) The alternative conformations of amyloidogenic proteins and their multi-step assembly pathways. *Curr. Opin. Struct. Biol. 8*, 101–106.
2. Pepys, M. B. (2006) Amyloidosis. *Annu. Rev. Med. 57*, 223–241.
3. Buxbaum, J. N., and Tagoe, C. E. (2000) The genetics of the amyloidoses. *Annu. Rev. Med. 51*, 543–569.
4. Colon, W., and Kelly, J. W. (1992) Partial denaturation of transthyretin is sufficient for amyloid fibril formation in vitro. *Biochemistry 31*, 8654–8660.
5. Lai, Z., Colon, W., and Kelly, J. W. (1996) The acid-mediated denaturation pathway of transthyretin yields a conformational intermediate that can self-assemble into amyloid. *Biochemistry 35*, 6470–6482.
6. Liu, K., Cho, H. S., Lashuel, H. A., Kelly, J. W., and Wemmer, D. E. (2000) A glimpse of a possible amyloidogenic intermediate of transthyretin. *Nat. Struct. Biol. 7*, 754–757.
7. Hammarstrom, P., Jiang, X., Hurshman, A. R., Powers, E. T., and Kelly, J. W. (2002) Sequence-dependent denaturation energetics: A major determinant in amyloid disease diversity. *Proc. Natl. Acad. Sci. U.S.A. 99* (Suppl. 4), 16427–16432.
8. Hammarstrom, P., Sekijima, Y., White, J. T., Wiseman, R. L., Lim, A., Costello, C. E., Altland, K., Garzuly, F., Budka, H., and Kelly, J. W. (2003) D18G transthyretin is monomeric, aggregation prone, and not detectable in plasma and cerebrospinal fluid: A prescription for central nervous system amyloidosis? *Biochemistry 42*, 6656–6663.
9. Jiang, X., Buxbaum, J. N., and Kelly, J. W. (2001) The V122I cardiomyopathy variant of transthyretin increases the velocity of rate-limiting tetramer dissociation, resulting in accelerated amyloidosis. *Proc. Natl. Acad. Sci. U.S.A. 98*, 14943–14948.
10. McCutchen, S. L., Colon, W., and Kelly, J. W. (1993) Transthyretin mutation Leu-55-Pro significantly alters tetramer stability and increases amyloidogenicity. *Biochemistry 32*, 12119–12127.
11. McCutchen, S. L., Lai, Z., Miroy, G. J., Kelly, J. W., and Colon, W. (1995) Comparison of lethal and nonlethal transthyretin variants and their relationship to amyloid disease. *Biochemistry 34*, 13527–13536.
12. Sekijima, Y., Hammarstrom, P., Matsumura, M., Shimizu, Y., Iwata, M., Tokuda, T., Ikeda, S., and Kelly, J. W. (2003) Energetic characteristics of the new transthyretin variant A25T may explain its atypical central nervous system pathology. *Lab. Invest. 83*, 409–417.
13. Sekijima, Y., Wiseman, R. L., Matteson, J., Hammarstrom, P., Miller, S. R., Sawkar, A. R., Balch, W. E., and Kelly, J. W. (2005) The biological and chemical basis for tissue-selective amyloid disease. *Cell 121*, 73–85.
14. Ferrao-Gonzales, A. D., Palmieri, L., Valory, M., Silva, J. L., Lashuel, H., Kelly, J. W., and Foguel, D. (2003) Hydration and packing are crucial to amyloidogenesis as revealed by pressure studies on transthyretin variants that either protect or worsen amyloid disease. *J. Mol. Biol. 328*, 963–974.
15. Shnyrov, V. L., Villar, E., Zhadan, G. G., Sanchez-Ruiz, J. M., Quintas, A., Saraiva, M. J., and Brito, R. M. (2000) Comparative calorimetric study of non-amyloidogenic and amyloidogenic variants of the homotetrameric protein transthyretin. *Biophys. Chem. 88*, 61–67.
16. Foss, T. R., Kelker, M. S., Wiseman, R. L., Wilson, I. A., and Kelly, J. W. (2005) Kinetic stabilization of the native state by protein engineering: implications for inhibition of transthyretin amyloidogenesis. *J. Mol. Biol. 347*, 841–854.
17. Hammarstrom, P., Schneider, F., and Kelly, J. W. (2001) Trans-suppression of misfolding in an amyloid disease. *Science 293*, 2459–2462.
18. Hammarstrom, P., Wiseman, R. L., Powers, E. T., and Kelly, J. W. (2003) Prevention of transthyretin amyloid disease by changing protein misfolding energetics. *Science 299*, 713–716.
19. Jiang, X., Smith, C. S., Petrassi, H. M., Hammarstrom, P., White, J. T., Sacchettini, J. C., and Kelly, J. W. (2001) An engineered transthyretin monomer that is nonamyloidogenic, unless it is partially denatured. *Biochemistry 40*, 11442–11452.
20. Johnson, S. M., Wiseman, R. L., Sekijima, Y., Green, N. S., Adamski-Werner, S. L., and Kelly, J. W. (2005) Native state kinetic stabilization as a strategy to ameliorate protein misfolding diseases: a focus on the transthyretin amyloidoses. *Acc. Chem. Res. 38*, 911–921.
21. Wiseman, R. L., Johnson, S. M., Kelker, M. S., Foss, T., Wilson, I. A., and Kelly, J. W. (2005) Kinetic stabilization of an oligomeric protein by a single ligand binding event. *J. Am. Chem. Soc. 127*, 5540–5551.
22. Quintas, A., Vaz, D. C., Cardoso, I., Saraiva, M. J., and Brito, R. M. (2001) Tetramer dissociation and monomer partial unfolding precedes protofibril formation in amyloidogenic transthyretin variants. *J. Biol. Chem. 276*, 27207–27213.
23. Hurshman, A. R., White, J. T., Powers, E. T., and Kelly, J. W. (2004) Transthyretin aggregation under partially denaturing conditions is a downhill polymerization. *Biochemistry 43*, 7365–7381.
24. Hornberg, A., Eneqvist, T., Olofsson, A., Lundgren, E., and Sauer-Eriksson, A. E. (2000) A comparative analysis of 23 structures of the amyloidogenic protein transthyretin. *J. Mol. Biol. 302*, 649–669.
25. Reixach, N., Deechongkit, S., Jiang, X., Kelly, J. W., and Buxbaum, J. N. (2004) Tissue damage in the amyloidoses: Transthyretin monomers and nonnative oligomers are the major cytotoxic species in tissue culture. *Proc. Natl. Acad. Sci. U.S.A. 101*, 2817–2822.
26. Sousa, M. M., Cardoso, I., Fernandes, R., Guimaraes, A., and Saraiva, M. J. (2001) Deposition of transthyretin in early stages of familial amyloidotic polyneuropathy: Evidence for toxicity of nonfibrillar aggregates. *Am. J. Pathol. 159*, 1993–2000.
27. Westermark, P., Sletten, K., Johansson, B., and Cornwell, G. G. (1990) Fibril in senile systemic amyloidosis is derived from normal transthyretin. *Proc. Natl. Acad. Sci. U.S.A. 87*, 2843–2845.
28. Benson, M. D. (1989) Familial amyloidotic polyneuropathy. *Trends Neurosci. 12*, 88–92.
29. Jacobson, D. R., Pastore, R. D., Yaghoubian, R., Kane, I., Gallo, G., Buck, F. S., and Buxbaum, J. N. (1997) Variant-sequence transthyretin (isoleucine 122) in late-onset cardiac amyloidosis in black Americans. *N. Engl. J. Med. 336*, 466–473.
30. Stangou, A. J., and Hawkins, P. N. (2004) Liver transplantation in transthyretin-related familial amyloid polyneuropathy. *Curr. Opin. Neurol. 17*, 615–620.
31. Miroy, G. J., Lai, Z., Lashuel, H. A., Peterson, S. A., Strang, C., and Kelly, J. W. (1996) Inhibiting transthyretin amyloid fibril formation via protein stabilization. *Proc. Natl. Acad. Sci. U.S.A. 93*, 15051–15056.
32. Razavi, H., Palaninathan, S. K., Powers, E. T., Wiseman, R. L., Purkey, H. E., Mohamedmohaideen, N. N., Deechongkit, S., Chiang, K. P., Dendle, M. T., Sacchettini, J. C., and Kelly, J. W. (2003) Benzoxazoles as transthyretin amyloid fibril inhibitors: Synthesis, evaluation, and mechanism of action. *Angew. Chem., Int. Ed. 42*, 2758–2761.
33. Adamski-Werner, S. L., Palaninathan, S. K., Sacchettini, J. C., and Kelly, J. W. (2004) Diflunisal analogues stabilize the native state of transthyretin. Potent inhibition of amyloidogenesis. *J. Med. Chem. 47*, 355–374.
34. Johnson, S. M., Connelly, S., Wilson, I. A., and Kelly, J. W. (2008) Biochemical and structural evaluation of highly selective 2-arylbenzoxazole-based transthyretin amyloidogenesis inhibitors. *J. Med. Chem. 51*, 260–270.
35. Coelho, T., Carvalho, M., Saraiva, M. J., Alves, I., Almeida, M. R., and Costa, P. P. (1993) A strikingly benign evolution of FAP in an individual found to be a compound heterozygote for two TTR mutations: TTR Met 30 and TTR Met 119. *J. Rheumatol. 20*, 179.

36. Deu, E., and Kirsch, J. F. (2007) The unfolding pathway for Apo *Escherichia coli* aspartate aminotransferase is dependent on the choice of denaturant. *Biochemistry 46*, 5810–5818.
37. Dev, S. K. N. D., Sinha, S., and Surolia, A. (2006) Thermodynamic analysis of three state denaturation of peanut agglutinin. *IUBMB Life 58*, 549–555.
38. Grimsley, J. K., Scholtz, J. M., Pace, C. N., and Wild, J. R. (1997) Organophosphorus hydrolase is a remarkably stable enzyme that unfolds through a homodimeric intermediate. *Biochemistry 36*, 14366–14374.
39. Hobart, S. A., Ilin, S., Moriarty, D. F., Osuna, R., and Colon, W. (2002) Equilibrium denaturation studies of the *Escherichia coli* factor for inversion stimulation: Implications for in vivo function. *Protein Sci. 11*, 1671–1680.
40. Hornby, J. A., Luo, J. K., Stevens, J. M., Wallace, L. A., Kaplan, W., Armstrong, R. N., and Dirr, H. W. (2000) Equilibrium folding of dimeric class μ glutathione transferases involves a stable monomeric intermediate. *Biochemistry 39*, 12336–12344.
41. Wiseman, R. L., Powers, E. T., Buxbaum, J. N., Kelly, J. W., and Balch, W. E. (2007) An adaptable standard for protein export from the endoplasmic reticulum. *Cell 131*, 809–821.
42. Lashuel, H. A., Wurth, C., Woo, L., and Kelly, J. W. (1999) The most pathogenic transthyretin variant, L55P, forms amyloid fibrils under acidic conditions and protofilaments under physiological conditions. *Biochemistry 38*, 13560–13573.
43. Pace, C. N. (1986) Determination and analysis of urea and guanidine hydrochloride denaturation curves. *Methods Enzymol. 131*, 266–280.
44. Hammarstrom, P., Jiang, X., Deechongkit, S., and Kelly, J. W. (2001) Anion shielding of electrostatic repulsions in transthyretin modulates stability and amyloidosis: Insight into the chaotrope unfolding dichotomy. *Biochemistry 40*, 11453–11459.
45. Fersht, A. R. (1999) *Structure and Mechanism in Protein Science*, W. H. Freeman and Company, New York.
46. Myers, J. K., Pace, C. N., and Scholtz, J. M. (1995) Denaturant m values and heat capacity changes: Relation to changes in accessible surface areas of protein unfolding. *Protein Sci. 4*, 2138–2148.
47. Schneider, F., Hammarstrom, P., and Kelly, J. W. (2001) Transthyretin slowly exchanges subunits under physiological conditions: A convenient chromatographic method to study subunit exchange in oligomeric proteins. *Protein Sci. 10*, 1606–1613.
48. Jacobson, D. R., McFarlin, D. E., Kane, I., and Buxbaum, J. N. (1992) Transthyretin Pro55, a variant associated with early-onset, aggressive, diffuse amyloidosis with cardiac and neurologic involvement. *Hum. Genet. 89*, 353–356.
49. Foss, T. R., Wiseman, R. L., and Kelly, J. W. (2005) The pathway by which the tetrameric protein transthyretin dissociates. *Biochemistry 44*, 15525–15533.
50. Wiseman, R. L., Powers, E. T., and Kelly, J. W. (2005) Partitioning conformational intermediates between competing refolding and aggregation pathways: Insights into transthyretin amyloid disease. *Biochemistry 44*, 16612–16623.

BI800636Q